Energy and Built Environment 3 (2022) 478–495

Contents lists available at ScienceDirect

Energy and Built Environment

journal homepage: http://www.keaipublishing.com/en/journals/energy-and-built-environment/

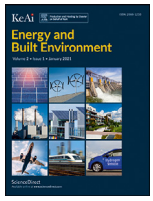

Efficacy of coupling heat recovery ventilation and fan coil systems in improving the indoor air quality and thermal comfort condition

Aminhossein Jahanbin

Department of Industrial Engineering (DIN), Alma Mater Studiorum - University of Bologna, Viale Risorgimento 2, 40136 Bologna, Italy

ARTICLE INFO

Keywords:
Heat recovery ventilation
Indoor air quality
Thermal comfort
Ventilation efficiency
Gaseous contaminants

ABSTRACT

Mechanical Ventilation with Heat Recovery (MVHR) systems are gaining increasing interest in buildings with low energy demand, for improvement of the Indoor Air Quality (IAQ) and reduction of the ventilation energy loss. In retrofitted buildings, MVHRs are often integrated with an additional air heater to cover space heating demand. Hence, evaluation of the interactions between MVHR and heat emitter, and their effects on indoor airflow characteristics is of significant importance. The present study aims to investigate effects of a combined MVHR-fan-coil system in heating mode on IAQ and thermal comfort parameters inside a retrofitted room, by means of a computational fluid dynamic (CFD) code. The proposed CFD model is validated by comparing the numerical results with experimental data. The results yielded by numerical simulations allow evaluating the indoor environmental quality characteristics as well as addressing the MVHR and fan coil interactions. The results indicate that the airflow discharged from the fan coil could have a significant impact on the age of the air; while it provides a desirable thermal comfort condition within the room, it may hinder to some extent delivery of the fresh air to the occupied zone due to creation of counterflow fields. Furthermore, it is shown that although increasing the fan speed (ON mode) would slightly enhance the air change efficiency, the OFF mode yields not only a better distribution of the fresh air but also a higher ventilation efficiency than when fan coil operates.

Introduction

Buildings account for 40% of the total energy consumption in Europe across the private and public sectors. European authorities have been planning substantial investment in recent years to improve energy efficiency in the present building stock, geared primarily to meet H2020 and the subsequent objectives [1]. Member of the European Union states are required to implement energy efficiency measures for buildings under the Directive on Energy Performance of Building [2]. Recent standards require high energy efficiency of buildings and remarkable efforts have been therefore made to improve insulation and airtightness of buildings. In such buildings, infiltration is low and mechanical ventilation systems are often used to achieve the required airflow [3].

The building ventilation has a significant impact on the energy performance, accounting for 30-60% of the energy use in buildings [4]. In fact, building ventilation manages the quantity of air required in the indoor space under specific environmental conditions. While higher ventilation rate inside a building zone would improve air quality and reduce pollutant concentration, it would consume more energy in the same time and create unpleasant indoor airflow causing discomfort to some occupants. Hence, a balanced solution requires to be considered.

MVHRs (Mechanical Ventilation with Heat Recovery) are ventilations with a heat recovery system, recovering the heat from exhaust air in order to reduce ventilation heat losses. MVHR system provides fresh filtered air into a building whilst retaining most of the energy that has already been used in heating the building. Moreover, they can be integrated with an additional air heater such as a fan coil or a low-temperature radiator to cover space heating demand. MVHRs are therefore gaining increasing interest in low energy and retrofitted buildings for improvement of indoor environmental quality, as well as reduction of ventilation energy losses.

In general, indoor environmental quality is co-determined by several environmental factors such as thermal comfort, Indoor Air Quality (IAQ), lighting, and acoustics. Previous studies have shown that the indoor environmental quality had a significant effect on human health, satisfaction, productivity, and effectiveness since people spend considerable amount of their time in indoor environments [5, 6]. Accordingly, it is necessary to investigate the impact of aforementioned factors on the assessment of indoor environmental quality.

In the context of IAQ, the effective distribution of fresh air within an occupied space is a crucial issue which is usually handled by the ventilation system. The IAQ depends on various parameters such as the ventilation system, number of people, indoor contaminants, and outdoor air conditions. Moreover, IAQ is also dependent on the nature of air movement within the envelope, as well as the nature and loca-

E-mail address: aminhossein.jahanbin@unibo.it

https://doi.org/10.1016/j.enbenv.2021.05.005
Received 31 December 2020; Received in revised form 10 May 2021; Accepted 11 May 2021
Available online 26 May 2021

Nomenclature

a	absorption coefficient (m^{-1})
ACH	air change efficiency (%)
c_p	heat capacity of air (J kg^{-1} K^{-1})
C	contaminant concentration (kg m^{-3})
$\widetilde{C}$	dimensionless contaminant concentration
D	diffusion coefficient (m^2 s^{-1})
DR	draught rate (%)
e	energy per unit mass (J kg^{-1})
$\dot{e}$	emission rate of contaminant sources (kg s^{-1})
E	strain rate (s^{-1})
f	compressibility factor / function
g	magnitude of the acceleration (m s^{-2})
G_f	volumetric fresh air (m^3 s^{-1})
h	specific enthalpy (J kg^{-1})
I	turbulence intensity
I_{cl}	clothing insulation (clo)
J	diffusion flux (kg m^{-2} s^{-1})
k	thermal conductivity (W m^{-1} K^{-1})
M	molar mass (kg mol^{-1})
$\dot{M}$	metabolic rate (met)
p	pressure (Pa)
PMV	predicted mean vote
PPD	percent person dissatisfied (%)
Re	Reynolds number
RH	relative humidity
S	source term
Sc	Schmidt number
T	temperature (K)
v	velocity magnitude (m s^{-1})
v_m	local mean velocity magnitude (m s^{-1})
V	volume (m^3)
VE	ventilation effectiveness
Q_{fan}	volume flow rate of fan coil (m^3 h^{-1})
x_v	molar fraction
$\bar{X}$	dimensionless parameter
y	horizontal coordinate / distance from wall (m)
Y	local mass fraction of species
U	thermal transmittance (W m^{-2} K^{-1})
z	vertical coordinate (m)

Greek symbols

α	thermal diffusivity (m^2 s^{-1})
β	thermal expansion coefficient (K^{-1})
ε	turbulence dissipation (m^2 s^{-3})
κ	turbulence kinetic energy (m^2 s^{-3})
μ	dynamic viscosity (kg m^{-1} s^{-1})
ξ	diffusion coefficient (m^2 s^{-1})
ρ	fluid density (kg m^{-3})
σ	Stefan-Boltzmann constant (W m^{-2} K^{-4})
τ	age of the air (s)
τ^*	dimensionless age of the air
$\bar{\tau}$	room-averaged age of the air (s)
$\bar{\tau}*$	dimensionless $\bar{\tau}$
$\tilde{\tau}$	shear stress (Pa)
Y	ventilation efficiency
φ	arbitrary scalar
Φ_{a-v}	air-to-vapour interaction parameter
Φ_{v-a}	vapour-to-air interaction parameter
ψ	factor related to air velocity
ω	filtering efficiency (%)
Ω	incident radiation (W m^{-2})

Subscripts

air	refers to air
ave	average value
bz	breathing zone
eff	effective value
exp	experimental
i	*i*-th
in	inlet
m	refers to moist air
mix	refers to mixture
num	numerical
opr	operative
out	outlet
oz	occupied zone
rad	refers to radiation
sv	refers to saturated vapour
t	refers to turbulence
v	refers to vapour
wall	refers to wall
win	refers to window
y	refers to distance from wall
0	reference value

tion of contaminants. In fact, IAQ could be affected by a number of pollutants such as Volatile Organic Compounds (VOCs), second-hand smoke, carbon monoxide, and biological particles (bioaerosols). The indoor contaminant is mainly classified into two types: aerosol particles and gaseous contaminants. High exposure of indoor pollutant may cause various health problem that would result into “sick building syndrome”.

Indoor air quality can be measured by absolute value of the contaminant concentration, ventilation effectiveness, and relative indicators such as age of the air [7]. The latter, namely the mean age of air (MAA), is an important parameter in assessing IAQ and the quality of ventilation. The local MAA is the averaged time of air molecules required to reach a certain location in the flow field [8]. Using this value, it is possible to determine the air change efficiency of the room, recommended for dwellings when no local source of contamination can be located, and at the same time, as a guarantee of desired air quality throughout the entire volume of the room [9].

Thermal comfort is another factor to be addressed in assessment of the indoor environmental quality. It is known that the quality of the thermal environment is the most essential factor in the indoor environment [10]. Thermal comfort depends not only on physical parameters, but also on psychological and physiological response of the human’s body to the environment. According to ASHRAE [11] and ISO 7730 [12], there are six primary factors that must be addressed when defining conditions for thermal comfort: metabolic rate, clothing insulation, air temperature, radiant temperature, air velocity and humidity. In general, thermal comfort is classified according to the type of environment: indoor, outdoor or semi-outdoor. In terms of indoor thermal comfort, the discussion centres mainly on two distinct approaches: classic steady-state model based on a heat balance model of human’s body [13], and adaptive model which is based on the field studies in naturally ventilated buildings [14].

To analyse indoor environmental quality, experiment is the common technique. Experimental analyses are reliable and has been widely employed in various indoor environments [15–19]. Nevertheless, acquisition of the required data to examine the indoor environmental quality is time-demanding and needs specific instruments [20]. Furthermore, complementary information on the domain under study such as spatial pressure/velocity distribution, prediction of streamlines, and turbulence statistics are not simply obtainable by experiments [21].

With rapid developments of numerical algorithms and computer sciences, an alternative technique to assess indoor airflow and hygrothermal characteristics of buildings is Computational Fluid Dynamic (CFD) method. Accordingly, several studies in recent years have employed CFD method to simulate and analyse the indoor air quality and thermal comfort condition in building sector [22–28]. For instance, a numerical analysis was carried out by Ning et al [24] on distribution of CO_2 and age of the air inside a bedroom. Effects of the different heights of conditioned air supply on air change efficiency and on CO_2 concentration in breathing zone were evaluated. They found that placing a supply fresh air at a lower level is effective in both saving energy and removing the exhaled CO_2.

Ye et al. [25] performed numerical simulations to investigate the distributions of aerosol particles and gaseous contaminant concentration inside a large-height space equipped with mixing ventilation and impinging jet ventilation systems. In another study, a comparative numerical study was carried out by Ganesh et al. [28] to assess the efficacy of two different radiators, namely double-panel radiator and ventilation radiator, in providing satisfying level of indoor environmental condition inside an office. They investigated airflow, thermal conditions, radiation temperature and turbulence intensity for two different geometric models and configurations.

Although CFD analyses have been abundantly employed to evaluate the thermal comfort condition in various environments, only few studies attempted to establish a comprehensive analysis on IAQ indices and thermal comfort parameters simultaneously. As an example, Chen et al. [26] investigated the air quality and thermal comfort of the kitchen environment by employing a finite volume CFD code. They investigated effects of exhaust volume on the particulate matter movement, age of the air, and comfort condition indices.

In literature, several studies can be found on performance of MVHR systems [29, 30]. However, they mainly aimed to analyse the airflow field and temperature distributions, as well as the energy consumption, without assessment of IAQ and thermal comfort condition. In particular, this gap is further for performance of coupled MVHR-heating systems and their effect on IAQ and thermal comfort. The present study aims to fill this gap by establishing a finite volume CFD code rendering possibility of simultaneous analysis of the turbulent airflow field characteristics and IAQ and thermal comfort indices for spaces conditioning with a combined heat recovery ventilation and fan coil system. The results yielded by the CFD model are validated against experimental data. The obtained results allow evaluating the local mean age of the air and distributions of gaseous contaminants concentration, i.e. VOCs and CO_2 concentrations, as well as the ventilation efficiency in removal of contaminants. Finally, impacts of the interaction between the heating system, namely the fan coil, and heat recovery ventilation unit on distribution of the fresh air, ventilation efficiency, and thermal comfort condition are addressed.

Methodology

Physical model, computational domain and boundary conditions

The domain under examination is a real case-study; a dormitory room of the student house located in Athens, Greece, undergone refurbishment with dimensions 5.31 m (x) × 5.22 m (y) × 2.70 m (z). The gross volume of the domain is 56.26 m^3 while the net volume is 49.17 m^3, obtainable by subtracting the bulk of furniture. The room domain consists of internal walls and only one external wall with large windows, where both MVHR and fan coil installed. The dormitory room has been furnished with 2 beds, a desk and chairs, two side-bed tables, and a large closet. The details and dimensions of the room components are illustrated in Fig. 1.

Since the room under study is a double-room, it is assumed that the room is occupied by two students. In order to have a precise evaluation of the air quality indices inside the domain, an occupied zone has been considered, presented in Fig. 1 by a rectangle with red dashed-line. In addition, 4 spots at beds and the desk have been selected, as the most likely occupied spots. These positions represent the breathing zones and are useful in accurate assessment of air quality and thermal comfort characteristics, shown in Fig. 1 with numbers 1 to 4 (henceforth p-1 to p-4). In order to take into account both reclining and sitting postures, positions p-1 and p-2 (beds) are evaluated at z=0.6 m, whereas p-3 and p-4 (desk) are evaluated at z=1.1 m.

Through the retrofitting process, the external wall has been insulated with the cross-laminated panels with mineral wool insulation, having thermal transmittance equal to U_{wall} = 0.33 W m^{-2} K^{-1}. Moreover, the single glazed windows have been replaced by a triple glazed type with low-emittance coating and spectral selective characteristics, with U_{win} = 0.81 W m^{-2} K^{-1}. More information on retrofitting process can be found in Ref. [31].

To evaluate the efficacy of the MVHR-Fan-coil system, the winter-heating condition was considered. The external temperature was assumed to be 5 °C, likely the minimum outdoor temperature for a typical winter day in Athens, Greece. The heating balance inside the room is affected by the heat losses through the external wall, windows and MVHR unit, and also by the heat gain from the fan coil and metabolic heat emitted by occupants. The latter was imposed inside the domain as heat sources equal to 70 W for each occupant [29]. Since the most undesirable condition is an overcast day in winter, the solar irradiation was ignored. The relative humidity for baseline simulations was adopted equal to 50%, whereas, for evaluation of the thermal comfort condition, various values of the relative humidity were employed in simulations ranging from 30 to 70%. In addition, the infiltration of outdoor air was ignored since the ventilation and air recirculation inside the room cause usually the positive pressure.

The employed MVHR system, integrated to external façade, is an energy saving system consists of a heat exchanger unit, filtering unit, and inlet and outlet vents with an identical cross-sectional area equal to 0.13 m × 0.02 m = 0.0026 m^2. It features a multi-layer filter allowing to reduce the indoor level of CO_2 and VOCs, and to eliminate the pollutants with dimension larger than 10 microns. The features of the employed MVHR system are presented in Fig. 2. The inlet supply air provides the fresh air perpendicular to inlet surface with volume flow rate equal to 30 m^3/h and thermal efficiency of 74%. The temperature of the air at supply inlet has been calculated by a UDF (User-Defined Function) code interpreted in the numerical model, taking into account the thermal efficiency of MVHR and the temperature at outlet vent.

A fan coil system with 0.9 m length, 0.29 m height and 0.23 m thickness has been installed horizontally on the surface of the external wall at height 2.3 m from the floor. The air flow exits at 45° direction from a supply vent with cross-sectional area of 0.032 m^2, with mean temperature 33.8 °C. The fan works with three different speed, providing air flow rates ranging from 349 to 510 m^3/h. For the preliminary analysis, the intermediate value of the flow rate was adopted, namely 427 m^3/h, equal to the inlet velocity 3.7 m/s. Then, for evaluating the impact of the fan coil performance on desired parameters, all flow rates as well as the OFF mode are taken into account.

As boundary conditions, the velocity inlet and outflow conditions were considered for inlets and outlets, respectively. The non-slip condition was imposed on all solid walls. The wall surfaces of the floor and ceiling were considered as adiabatic, while the internal walls were assumed to be isothermal, with the wall temperature value equal to 20 °C. The boundary condition of the third kind was imposed at the external wall and windows. The following values of thermal transmittance for the external wall and windows were considered, respectively: U_{wall} = 0.33 W/(m^2K) and U_{win} = 0.81 W/(m^2K), equal to those reported above for the room after retrofitting process. The furniture and other existing solid walls, including the case of the MVHR and fan coil, were assumed as adiabatic. The corresponding boundary conditions of the mean age of the air, VOCs transport, and CO_2 distribution are discussed in details in their relevant sections.

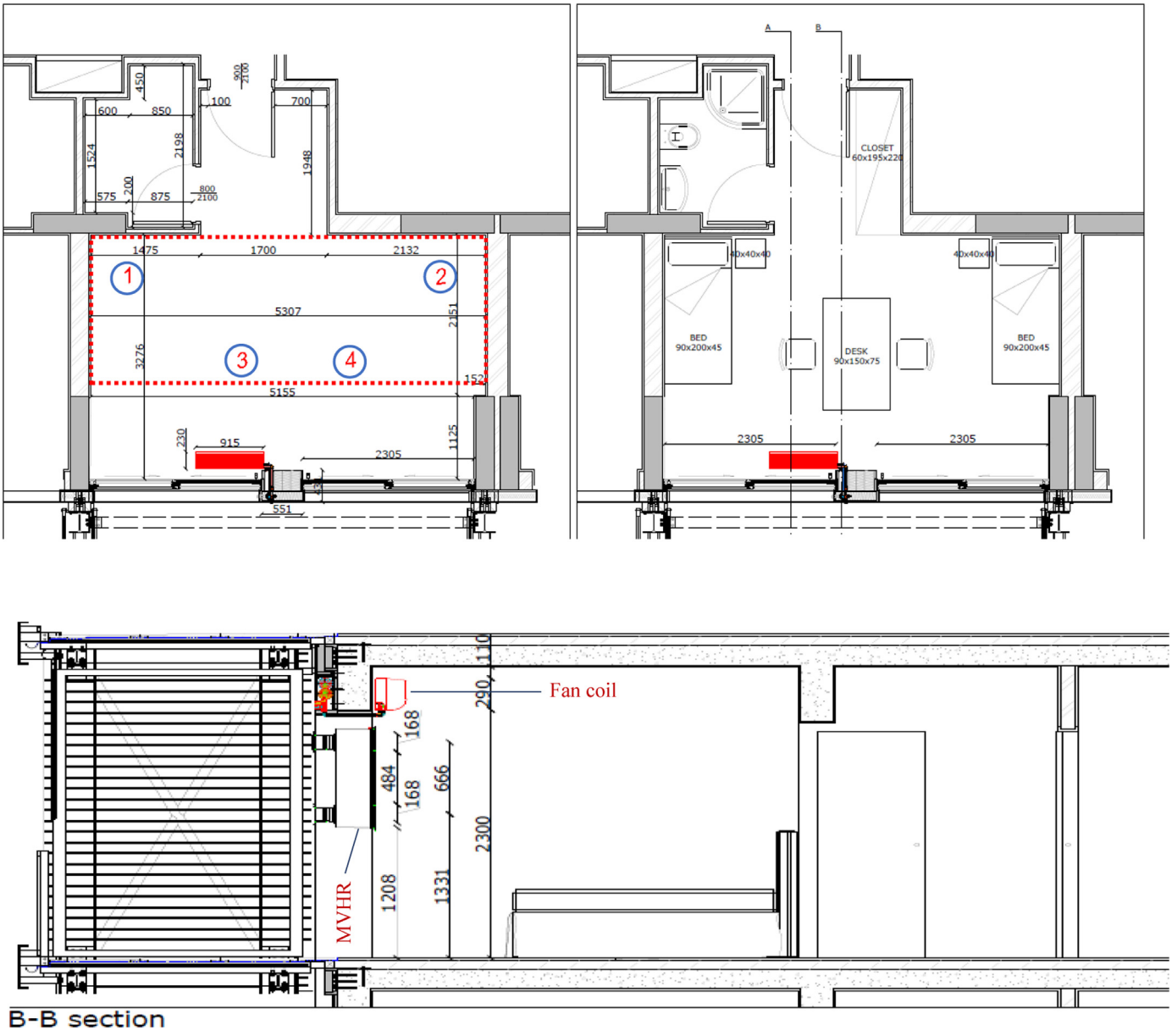

Fig. 1. Plan of the dormitory room.

Finite volume CFD code

The indoor airflow is a turbulent flow which is driven by momentum and buoyancy force. Considering the low air velocity as well as the small gradient of the pressure, the flow was supposed to be incompressible. It was assumed that the thermophysical properties are constant except the density, varying linearly with temperature. Since temperature differences inside the room are rather small, the Boussinesq approximation was employed to consider the buoyancy effect. For simulation of airflow fields, the indoor air was assumed as the humid air and the corresponding thermal properties were evaluated at relative humidity of 50%, presented in Section 2.4. The steady-state governing equations for mass, momentum and energy are given by:

$$\nabla \cdot \vec{v} = 0 \tag{1}$$

$$\rho_0(\vec{v} \cdot \nabla)\vec{v} = -\nabla(p + \rho_0 g z) + \rho_0 g \beta (T - T_0)\nabla z + \nabla \cdot \tilde{\tau}_{eff} \tag{2}$$

$$\nabla \cdot (\vec{v}(\rho e + p)) = \nabla \cdot \left[(k + k_t)\nabla T + \tilde{\tau}_{eff} \cdot \vec{v}\right] \tag{3}$$

where β is the air thermal expansion coefficient, $\tilde{\tau}_{eff}$ is the effective stress tensor defined as $\tilde{\tau}_{eff} = \tilde{\tau} + \tilde{\tau}_t$, where in the Boussinesq approximation $\tilde{\tau} = \mu(\nabla\vec{v} + \nabla\vec{v}^T)$ and $\tilde{\tau}_t = \mu_t(\nabla\vec{v} + \nabla\vec{v}^T)$. The turbulent dynamic viscosity, μ_t, and turbulent thermal conductivity, k_t, are determined through the turbulence model.

Furthermore, e is the energy per unit mass and is given by:

$$e = h - \frac{p}{\rho} + \frac{v^2}{2} \tag{4}$$

where h is the specific enthalpy.

The 3D governing differential equations were solved by means of finite volume method implemented through the CFD code ANSYS Fluent. A second-order upwind scheme was adopted in order to convert the governing equations into a set of algebraic discretized equations and the Semi-Implicit Method for Pressure-Linked Equation (SIMPLE) was utilised to solve the pressure-velocity coupling. The convergence of The CFD solutions was monitored by controlling the history of residuals, representing the differences in the value of the desired quantity between two iterations. In order to optimize the solution convergence, under-

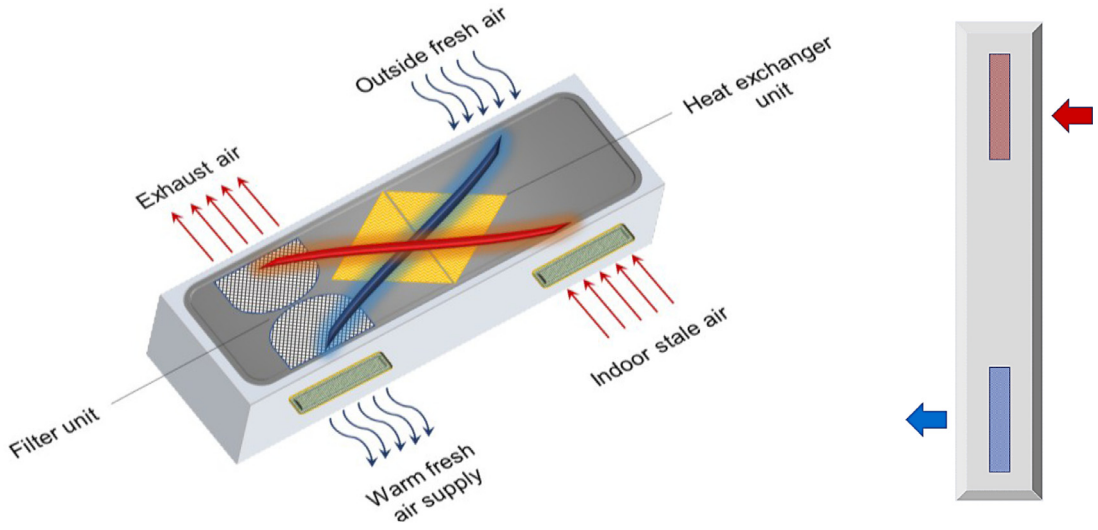

Fig. 2. Features of the MVHR system (left) and its lateral view (right).

Table 1
Constants and parameter adopted in the turbulence model.

$C^*_{1\varepsilon}$	η	η_0	γ	C_μ	$C_{1\varepsilon}$	$C_{2\varepsilon}$	α_k	α_ε
$C_{1\varepsilon} - \frac{\eta(1-\eta/\eta_0)}{1+\gamma\eta^3}$	$\sqrt{2E_{ij}E_{ij}}\frac{\kappa}{\varepsilon}$	4.377	0.012	0.0845	1.42	1.68	1.39	1.39

relaxation factors for momentum and turbulence terms were utilised. As a final check of the solution accuracy, the balance of heat flow through the domain boundaries was considered.

Turbulence modelling

The RNG (Renormalisation Group) k-ε turbulence model was employed in this study, due to its higher stability and precision rendering for internal flows [32, 33]. The RNG model is quite similar to the classic κ-ε model, but includes some improvements such as an additional term in ε to enhance the accuracy and a differential formula for the effective-viscosity accounting for low-Reynolds numbers effects [33]. The governing equations for RNG κ-ε model are given by [34]:

$$\nabla \cdot \left(\rho K \vec{v}\right) = \nabla \cdot \left(\alpha_\kappa \mu_{eff} \nabla K\right) + 2\mu_t E_{ij} E_{ij} - \rho\varepsilon \tag{5}$$

$$\nabla \cdot \left(\rho\, \varepsilon\, \vec{v}\right) = \nabla \cdot \left(\alpha_\varepsilon \mu_{eff} \nabla \varepsilon\right) + C^*_{1\varepsilon} \frac{\varepsilon}{\kappa} 2\mu_t E_{ij} E_{ij} - C_{2\varepsilon} \rho \frac{\varepsilon^2}{\kappa} \tag{6}$$

where E_{ij} is the strain rate. The values of μ_{eff} and μ_t are defined as:

$$\mu_{eff} = \mu + \mu_t\,; \quad \mu_t = \rho C_\mu \frac{\kappa^2}{\varepsilon} \tag{7}$$

Corresponding values of the turbulence model's constants are reported in Table 1.

The enhanced wall treatment method was adopted in this study in order to model near-wall turbulent flow. This method is based on the turbulent Reynolds number, $Re_y = \rho\, y\, k^{0.5} \mu^{-1}$, combining a viscosity-affected layer and fully turbulent region (two-layer model). Furthermore, at inlet vents, the value of the turbulence intensity was assumed to be 5% and the turbulent viscosity ratio was considered equal to 10.

Thermophysical properties

The thermophysical properties of moist air were adopted in this study since the air inside the room is a moist air. The thermophysical properties of humid air were determined by utilizing the expressions proposed in [35]. The density, specific heat capacity, thermal conductivity, and viscosity of the humid air were determined through the following correlations:

$$\rho_m = \frac{1}{z_m(x_v, T)} \frac{p_0}{RT} M_a \left[1 - x_v \left(1 - M_v/M_a\right)\right] \tag{8}$$

$$c_{p_m} = c_{p_a} x_a \frac{M_a}{M_m} + c_{p_v} x_v \frac{M_v}{M_m} \tag{9}$$

$$\kappa_m = \frac{\left(1 - x_v\right)\ \kappa_a}{\left(1 - x_v\right) + x_v\ \Phi_{a-v}} + \frac{x_v\, \kappa_v}{x_v + \left(1 - x_v\right)\Phi_{v-a}} \tag{10}$$

$$\mu_m = \frac{\left(1 - x_v\right)\ \mu_a}{\left(1 - x_v\right) + x_v\ \Phi_{a-v}} + \frac{x_v\ \mu_v}{x_v + \left(1 - x_v\right)\Phi_{v-a}} \tag{11}$$

where M is the molar mass, z_m is the enhancement factor equal to 0.9987 for 20°C, and x_v is the molar fraction of water vapour and is obtained by:

$$x_v = f(P,T)\ RH\ \frac{p_{sv}}{p_0} \tag{12}$$

where f is the compressibility factor, equal to 1.001 for 20°C, and RH is the relative humidity considered equal to 50%. In Eq. (10 and 11), $\Phi_{a-v}$is the interaction parameter between air and water vapour and $\Phi_{v-a}$is the interaction parameter between vapour and air, which can be calculated through equations provided in [35]. Furthermore, thermal properties of dry air at atmospheric pressure were taken from Ref. [36].

The fluid density ρ was assumed to be constant except in the buoyancy force term, which is estimated by the Boussinesq approximation as a linear function of the temperature:

$$\rho = \rho_0 \left[1 - \beta\left(T - T_0\right)\right] \tag{13}$$

The corresponding values of the properties of moist air, obtained for reference temperature, T_0 = 20°C, are reported in Table 2.

Radiation model and operative temperature

Radiation heat transfer in numerical model was taken into account by applying a model expanding the radiative transfer equation into an

Table 2
Thermophysical properties of the moist air.

ρ [kg m^{-3}]	c_p [J kg^{-1} K^{-1}]	k [W m^{-1} K^{-1}]	μ [kg m^{-1} s^{-1}]	β [K^{-1}]
1.153	1019	0.0253	1.82×10^{-5}	0.00341

orthogonal series of spherical harmonics. It solves a simple diffusion equation for the incident radiation Ω. The equation of the adopted radiation model can be given as:

$$\nabla.q_{rad} + a\Omega = 4an^2\sigma T^4 \tag{14}$$

where a is absorption coefficient, n is rarefactive index, and σ is Stefan-Boltzmann constant. This expression is directly substituted into the energy equation to account for heat sources/sinks due to radiation. The solid surfaces are assumed to be diffusive and grey and values of the internal emissivity were selected similar to those employed in [33].

The operative temperature, T_{opr}, is associated to combined effects of convective and radiant heat transfer and is determined through Eq. (15), according to ISO 7730 [12]:

$$T_{opr} = \psi T_{air} + (1-\psi)T_{rad} \tag{15}$$

where ψ is a weight factor depending on the air velocity and assumed equal to 1/2. The mean radiant temperature is the most important parameter governing human energy balance, with the strongest impact on thermo-physiological comfort indexes such as physiological equivalent temperature (PET) or predicted mean vote (PMV). The mean radiant temperature, T_{rad}, is obtainable by solving Eq. (14).

Evaluation of thermal comfort

Although a number of measuring parameters for evaluation of thermal comfort are currently available, the most common and classical parameters are the Predicted Mean Vote (PMV) and the corresponding Percent Person Dissatisfied (PPD) [20, 37]. The PMV index predicts the mean value of the subjective ratings of a large group of occupants exposed to the same environment, and is expressed by a seven points thermal sensation scale between -3 and +3 (cold to hot). The PPD quantitatively predicts the percentage of thermally dissatisfied occupants. PMV index can be assessed as a function of four environmental variables, namely air temperature T_{air}, mean radiant temperature T_{rad}, air velocity v_{air}, and air humidity RH, and of the person's metabolic rate $\dot{M}$ as well as the clothing insulation I_{cl}. Therefore, it can be expressed as:

$$\mathrm{PMV} = f\left(T_{air}, T_{rad}, v_{air}, RH, \dot{M}, I_{cl}\right) \tag{16}$$

The corresponding equations and relevant parameters to calculate the PMV index can be found in [12], not reported here for the sake of brevity. The PPD is calculated by an empirical relationship, based on experimental studies in which participants voted on their thermal sensation:

$$\mathrm{PPD} = 100 - 95\exp\left(-0.3353\mathrm{PMV}^4 - 0.2179\mathrm{PMV}^2\right) \tag{17}$$

In the present study, to evaluate values of PMV and PPD, a MATLAB code has been developed acquiring the relevant data from numerical simulation. For solving the heat balance equation to estimate the temperature of occupants' clothes, an iterative method has been utilised. The value of clothing insulation was adopted as 1.0 clo, a typical value of winter clothing. Two metabolic rates were considered, namely 0.9 met (at p-1 and p-2) and 1.2 met (at p-3 and p-4), taking into account the metabolic rate for both reclining and sitting postures. Furthermore, in assessment of the thermal comfort condition, the local thermal discomfort caused by the draught rate, vertical air temperature difference, radiant temperature asymmetry, and floor surface temperature have been taken into account.

Transport model for age of the air

The fresh air from the supply inlet flows to an arbitrary point inside the domain via various pathways. The air or a contaminant can also reach the outlet via various routes. Hence, the air must be described statistically. Local mean age of the air is a statistical value addressing the time that all particles of fresh air require to move from supply inlet to an arbitrary point. The age of the air is an important index identifying the air quality; the younger the age of the air, the better quality of indoor air.

To analyse the local mean age of the air, a User-Defined Scalar (UDS) has been incorporated into the CFD model in the pre-processing stage. In order to calculate the transport of an arbitrary scalar φ_i, one additional convection-diffusion equation was solved, expressed as:

$$\nabla.\left(\rho\vec{v}\varphi_i - \xi_i\nabla\varphi_i\right) = S_{\varphi_i} \tag{18}$$

where ξ_i and S_{φ_i} are the diffusion coefficient and source term of the scalar φ_i. The latter is usually set as a fixed value, i.e. $S_{\varphi_i} = 1$. The diffusion term ξ_i has been compiled in numerical code via a UDF to account for turbulent diffusion. It can be calculated from the effective viscosity of the air μ_{eff} and is determined as [38]:

$$\xi_i = \left(2.88\times10^{-5}\right)\rho + \frac{\mu_{eff}}{Sc_t} \tag{19}$$

where Sc_t is the turbulent Schmidt number. The boundary conditions for the solution of Eq. (18) are a zero gradient at air outlets and at solid wall surfaces, and a zero value at air supply inlet [39].

When defining the boundary condition for the solution of Eq. (18), the main challenge is to define a correct value of the age of the air at fan coil inlet. Since the fan coil recirculates the air handed over at outlet vent, setting the zero value (as fresh air supply inlet) or zero gradient (as walls) leads to the unrealistic results. In this case, the correct value of the boundary condition at fan coil inlet should be equal to the mean age of the air at fan coil outlet. To perform that, another UDF was written in the CFD code which obtains the mean age of the air at outlet for $(i\text{-}1)_{th}$ iteration and sets it up as the boundary condition value at inlet for $(i)_{th}$ iteration.

Modelling of the gaseous contaminants

In the present study, VOCs, namely formaldehyde and toluene, as well as CO2 are regarded as representative of the indoor gaseous contaminants. In order to simulate the emission and transport of contaminants inside the room, the species transport model was applied. This model can predict the mixing and transport of chemical species by solving conservation equations describing convection, diffusion, and reaction sources for each component species. The conservation equation for species transport takes the following general form:

$$\nabla.\left(\rho\vec{v}Y_i\right) = \nabla.\vec{J}_i + S_i \tag{20}$$

where Y_i is the local mass fraction of each species, $\vec{J}_i$ is the diffusion flux of species i, and S_i is the source term including the rate of creation and also the net rate of production by chemical reaction of species. The mass diffusion in turbulent flow was determined through the equation below:

$$\vec{J}_i = -\left(\rho D_{i,mix} + \frac{\mu_t}{Sc_t}\right)\nabla Y_i \tag{21}$$

where $D_{i,mix}$ is the diffusion coefficient for species i in the mixture.

For the mixture species, the density was determined by considering the mixture as an incompressible ideal-gas while the specific heat at constant pressure was estimated by mixing-law. It was also assumed that species undergo no chemical reaction or transformation during the diffusion process and move along with the indoor air at the same velocity.

Volatile organic compounds (VOCs) are prevalent indoor air pollutants, with primary sources typically consumer products and building

materials. Building materials, such as engineered wood products, coatings, and painted walls may emit numerous VOCs, including formaldehyde and toluene. Such hazardous air pollutants are up to an order of magnitude higher indoors than outdoors, particularly in renovated spaces [40].

The VOCs emission inside the computational domain has been taken into account by presenting the formaldehyde and toluene as the main contaminants. It was supposed that formaldehyde is emitted from the wooden materials comprising the beds, bedside tables and desk, whereas toluene is considered as the contaminant emitted from the painted surrounding walls. It was found that different furniture materials may have different emission rates of formaldehyde with different orders of magnitude [41]. The emission rate of formaldehyde from furniture was considered equal to 0.02 mg/(m^2h), as suggested in Ref [42], with total emitting area equal to 4.60 m^2.

For the case of toluene, it was assumed that toluene is emitted from vertical walls of the room. The emission rate of the toluene was set equal to 0.056 $\mu g/(m^2 s)$ [43], with 31.6 m^2 total emission area. Moreover, it was assumed that formaldehyde and toluene have a zero value at inlet of supply air and have a zero gradient at outlets and wall surfaces.

On the other side, the main source of CO_2 in an occupied space is exhalation of occupants. Although CO_2 is not solely considered as a significant health risk to occupants, the CO_2 concentration is considered as an indicator for evaluation of the ventilation efficiency. In the present study, the CO_2 released from occupants is introduced inside the domain via two small elliptical surfaces above beds representing the occupants' mouths. The emission rate of CO_2 was set to 0.01 g/s for each occupant, which is slightly higher than the emission rate employed in Ref. [43]. In addition, the exhaled air temperature was assumed to be 34 °C [25].

The concentration of the CO_2 at supply inlet was calculated by taking into account the outdoor CO_2 concentration C_{out}, namely the background CO_2, as well as the filtering efficiency of the MVHR unit ω. The concentration of the CO_2 at supply inlet, $C_{in,}$ is given by:

$$C_{in} = (1 - \omega/100) \times C_{out} \tag{22}$$

The outdoor CO_2 level was considered equal to 0.70 g/m^3, i.e. 350 ppm. Moreover, the filtering efficiency of the MVHR unit in reducing the CO_2 level is 10%. The CO_2 concentration at supply inlet vent of the fan coil system was consider equal to the CO_2 concentration at outlet vent of the fan coil since the air is recirculated. Furthermore, for CO_2 transport equation, a zero gradient boundary condition was assumed at all wall surfaces inside the domain.

Model validation

Grid generation and mesh independence analysis

The polyhedral cells were used to generate the grid of the computational domain. The computational domain was preliminary meshed with tetrahedral elements, containing 3 634 258 cells. A non-uniform grid strategy was applied; a higher mesh density around the inlets, outlets, and solid walls and a lower mesh density with expansion rate for far field regions. Then, the tetrahedral mesh was converted to polyhedral mesh in order to enhance the grid quality. The major benefit of the polyhedral grid is that each individual cell has many neighbours and, therefore, gradients can be much better estimated in comparison to tetrahedral grid. The final polyhedral mesh selected for the simulation has 760 145 elements with 4 205 926 nodes, illustrated in Fig. 3.

Grid independence check was worked out to ensure the accuracy of the numerical model. For indoor environment, as recommended by Chen and Srebic [44], a good practice for verification of the numerical model is to refine systematically the grid size by doubling the grid elements number and to compare the corresponding results. To prove that, a grid was generated with almost 2 times finer elements than the selected mesh for final computations, namely Mesh 1. The simulations were performed for the baseline model under the same conditions. In order to have an accurate comparison and to examine all regions inside the domain, the mean value of variables on the diagonal line, connecting two corners of the domain, has been compared.

Table 3
Grid independence.

			v	T_{opr}	I_{turb}
Mesh	No. poly cells	No. nodes	[m s^{-1}]	[°C]	[°C]
1	760 145	4 205 926	0.287	21.68	5.63
2	1 467 079	6 719 472	0.293	21.56	5.71
Discrepancy [%]			1.95	0.56	1.42

Table 3 compares the mean values of the air velocity, air temperature, radiant temperature, operative temperature and turbulence intensity on the diagonal line, obtained by both meshes. The table shows that the discrepancy between the results obtained by finer mesh and those obtained by the selected mesh for final computation is insignificant. It is therefore confirmed that the chosen grid density is adequate and the results are meh independent.

Validation of airflow model

In order to validate the numerical code, the results obtained by numerical simulations were validated against the measured data. To prove that, two separate validation were worked out, presented in the following.

The numerical model employed for prediction of the turbulent airflow fields inside the room is validated by comparison with experimental measurements performed to determine the airflow velocity. An air velocity meter, to be more precise a handheld anemometer, with accuracy ±0.015 m/s was utilized to measure the air velocity in centreline of the room at various distances from the fan coil (y direction) and different height from the floor (z direction). For better interpretation of the air velocity at various points, a dimensionless parameter $\bar{X} = z/y$ has been defined, representing the ratio of the height to distance from the fan coil. Since the values of the air velocity in far-field (from the fan coil) are too low, the speed of fan was set to maximum value, with inlet air velocity equal to 4.4 m/s.

The comparison between the measured data and numerical results are presented in Fig. 4. The figure shows that, except of the $\bar{X} = 3.34$ with 0.1 m/s difference, the simulation results are in good agreement with experimental data. To evaluate the discrepancy between the measured data and simulation results, the Root-Mean-Square-Deviation (RMSD) was analysed. For an arbitrary variable φ, the RMSD is defined as:

$$RMSD = \sqrt{\frac{\sum_{i=1}^{N} \left(\left[\varphi_{Exp}\right]_i - \left[\varphi_{Num}\right]_i \right)^2}{N}} \tag{23}$$

The mean square deviation between values of the air velocity yielded by measurement and those obtained by numerical simulation is equal to 0.05 m/s.

Validation of contaminant concentration/transport model

To validate the reliability of the employed numerical model for contaminant distribution, profiles of the CO_2 concentration obtained by numerical model are compared with those obtained by experimental data given in Ref. [43]. The experiments were conducted in a test chamber with a size of 3.9 m (x) × 2.9 m (y) × 2.6 m (z), ventilated via a 0.2 m × 0.17 m rectangular air grille and a 0.6 m × 0.6 m perforated ceiling exhaust with 15.3% as the effective area ratio. The supply air at grille flows with velocity equal to 1.19 m/s velocity and temperature of 19 °C. CO_2 is released via a small hole of 10 mm bore at the height of 1.1 m with an initial velocity of 0.039 m/s in horizontal direction, representing the exhalation from the occupant.

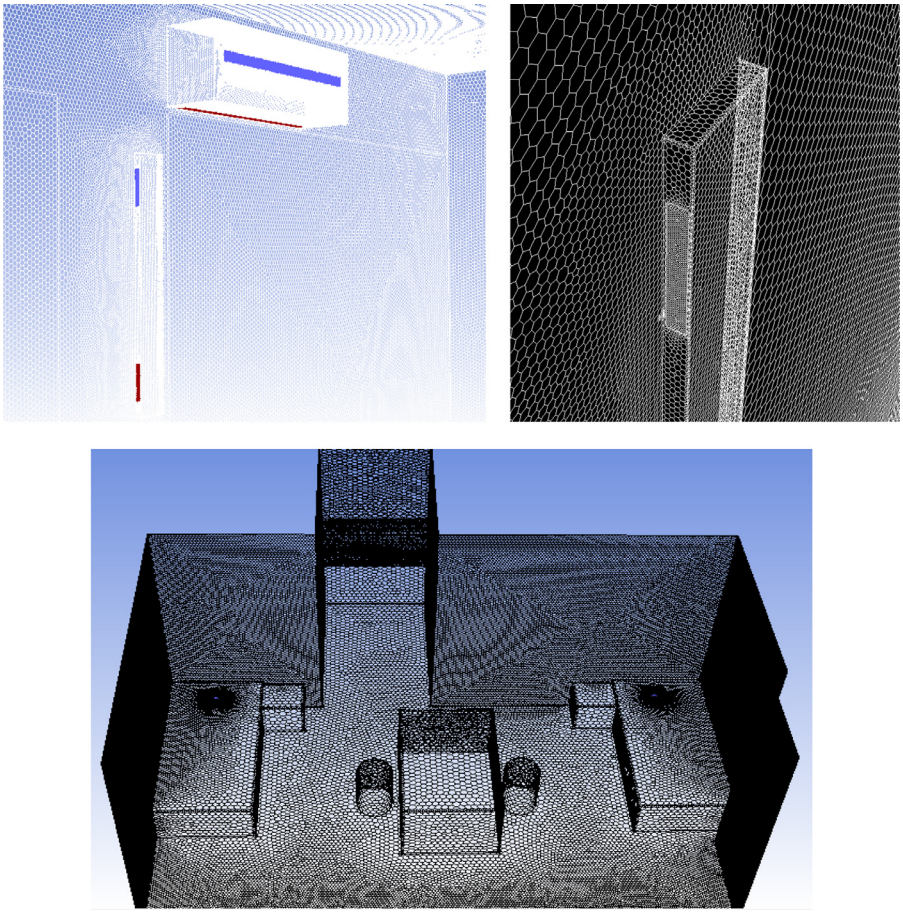

Fig. 3. Parts of the surface mesh employed for the numerical model (left); monochromic view of the grid density in vicinity of the inlet/outlet vent (right); the employed mesh for walls/furniture (bottom).

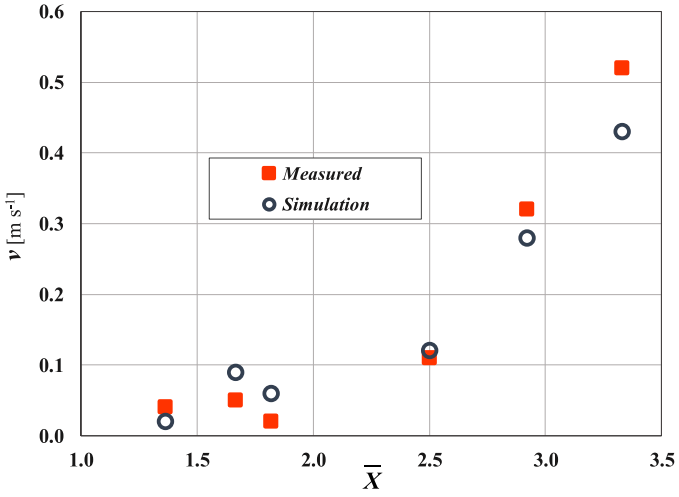

Fig. 4. The comparison between the measured and simulated values of the air velocity at different positions.

The multi-point non-dispersive infrared CO_2 system was used to measure the concentration of CO_2. The measuring range is 0 ppm to 2000 ppm and the measuring error is ±20 ppm, with dynamic responding time less than 60 s. The results were presented in various plumb lines, i.e. positions with fixed values of x and y varying from floor to ceiling (z direction). Furthermore, for the model validation, an additional numerical model with geometry and specifications similar to the test chamber was provided, employing exactly the same CFD model as that presented in Section 2.

Table 4
Mean square deviation of numerical results from experimental data for different plumb lines.

	Plumb Line				
	I	**II**	**III**	**IV**	Median
RMSD [ppm]	37.6	57.4	60.1	39.4	48.6

Comparisons between the measured and simulated values of CO_2 concentration for locations along Plumb Lines "I - IV" are illustrated in Fig. 5. The figure shows that the simulated CO_2 concentration profiles are in satisfying agreement with experimental data. Considering the measuring error of ±20 ppm, the point-to-point discrepancy between the simulation results and measured data is acceptable. In addition, part of the discrepancy between results may be attributed to the background CO_2 concentration in test chamber, which was not mentioned explicitly in the experiment descriptions. Mean square deviation of the simulation results from experimental data for different plumb lines were reported in Table 4.

Results and discussion

Airflow fields and operative temperature distribution

The distribution of the air velocity and temperature obtained by numerical simulation allows to understand the physical behaviour of any type of the flow inside the enclosure. The streamlines coloured by the velocity magnitude and the operative temperature distributions, at a

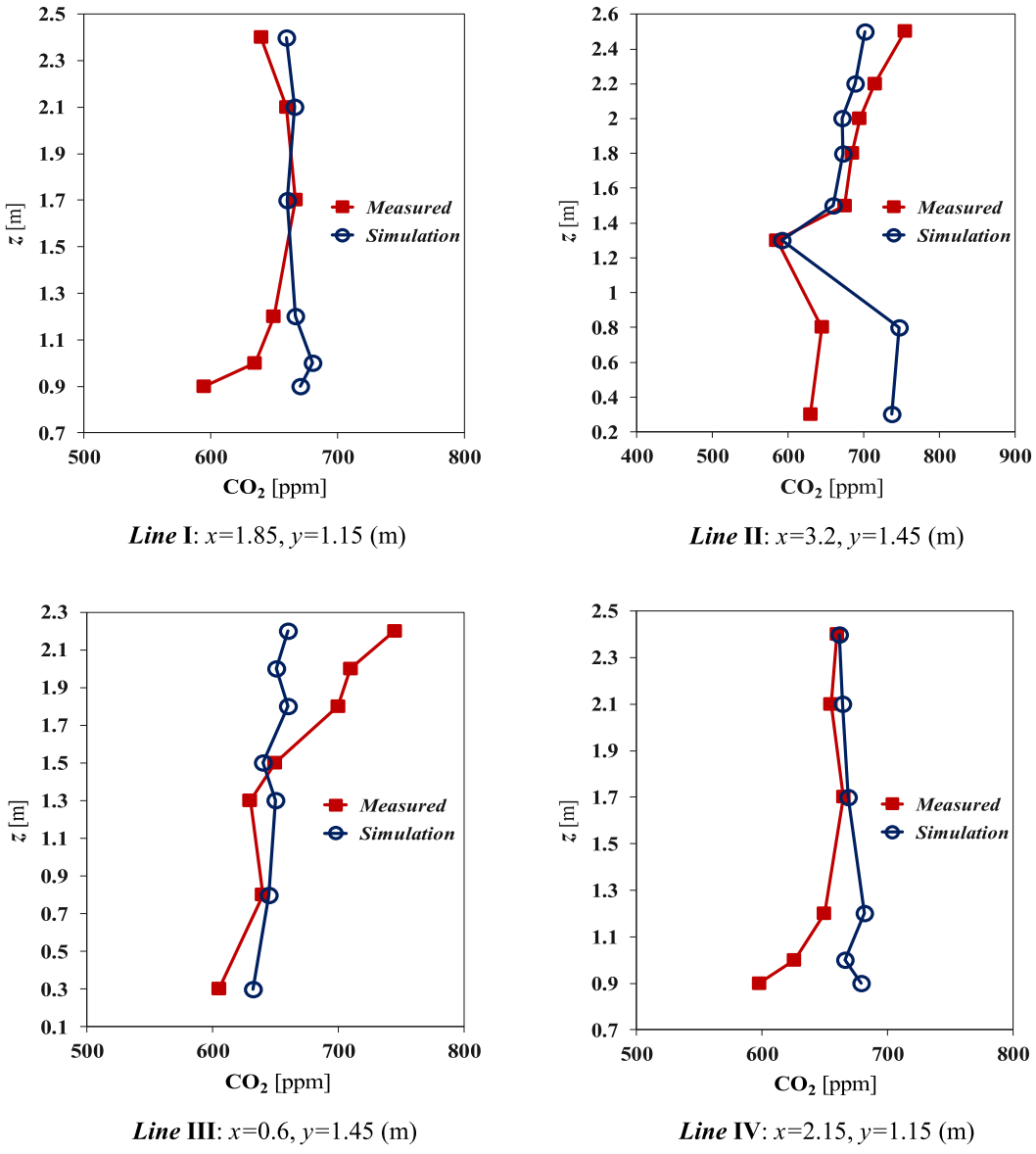

Fig. 5. CO_2 concentration profiles for various positions in ppm: measured vs. simulated.

horizontal plane at z=1.1 m, are illustrated in Fig. 6. The figures show that the fan coil stream affects to significant extent both velocity and temperature profiles; the left-hand side of the room, undergone the separated flow zones with diverse eddies, has a higher velocity magnitude and temperature. On the other hand, except of the near wall zone, the right-hand side of the domain has a quasi-uniform distribution of the velocity and operative temperature, with an average velocity magnitude and operative temperature equal to 0.07 m/s and 21.7 ˚C, respectively. Furthermore, in vicinity of the MVHR unit and the right-side window, small vortexes with a rather lower operative temperature can be observed.

Fig. 7 displays the streamlines and operative temperature distributions on vertical sectional planes at distances of 1 m and 3 m from the external wall, namely y=1 m and y=3 m. The figure shows that the airflow jet after exhausting from the fan coil reaches the front wall, before flowing along the wall and towards the ceiling. Such stream transfers the heat and results into having a rather high temperature zone for the left-hand side of the room. For the right side of the room, the stratification of the operative temperature from floor to ceiling is evident, with a varying range from 20.4 ˚C to 22.5 ˚C.

For the zone in front of the fan coil, the vertical planes show that the forced convection condition is prevalent. The vertical plane, at y=1 m, demonstrates a plume in front of the fan coil, with velocity magnitude around 0.8 m/s, while another vertical plane, at y=3m, shows a slight increase of the air velocity and temperature with height, which is mainly due to the buoyancy force. In addition, for both sectional planes, a rather high air velocity near walls can be observed.

To show better the distribution of air velocity discharged from the fan coil, Fig. 8 illustrates streamlines and air velocity magnitude on the vertical sectional plane (y-z) crossing the fan coil inlet vent. The figure apparently shows that the discharged air from the fan coil moves around 2 m under forced convection condition before ascending towards the ceiling due to the higher temperature and buoyancy. Figure shows that this airflow causes two large vortices; one alongside of the airflow jet and another in the upper-right corner of the room.

Profiles of the air temperature and velocity at occupied positions, namely p-1 to p-4, marked in Fig. 1, are illustrated in Figs. 9 and 10. The figures show the variation of the air temperature and velocity with height, from z=0.6 to z=2 m. It can be observed that p-1 and p-3 render a higher air temperature at any heights than p-2 and p-4 since the

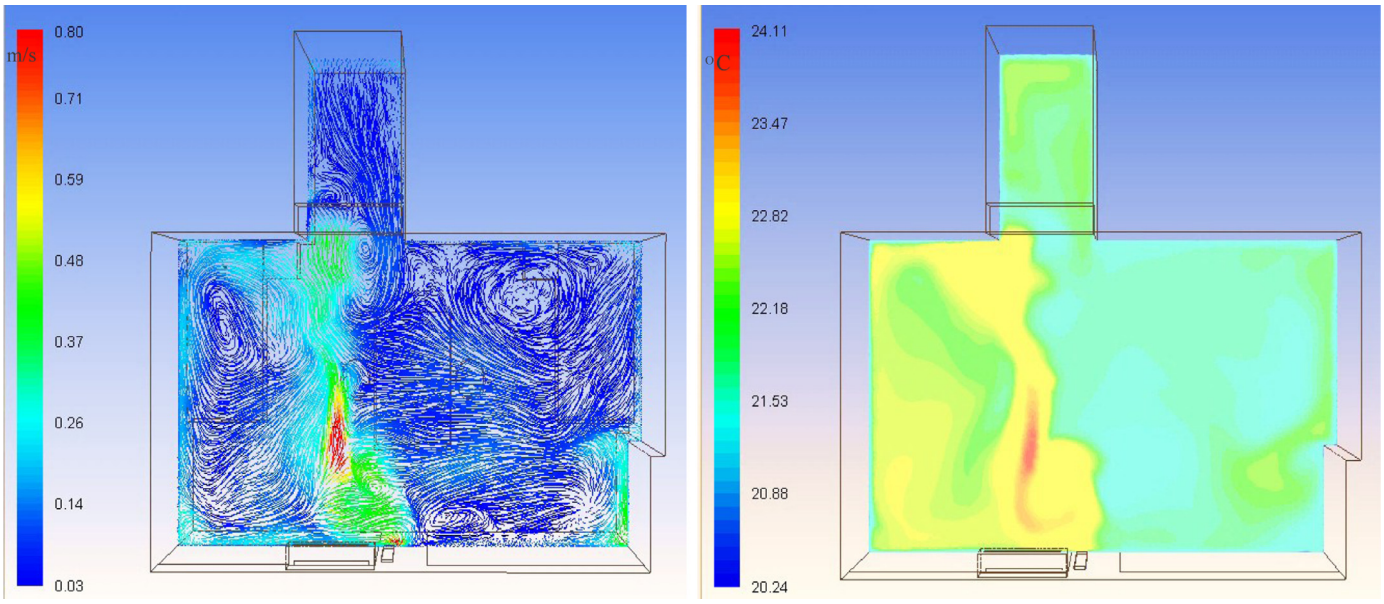

Fig. 6. Streamlines (left) and operative temperature distributions (right) on the horizontal plane at z=1.1 m.

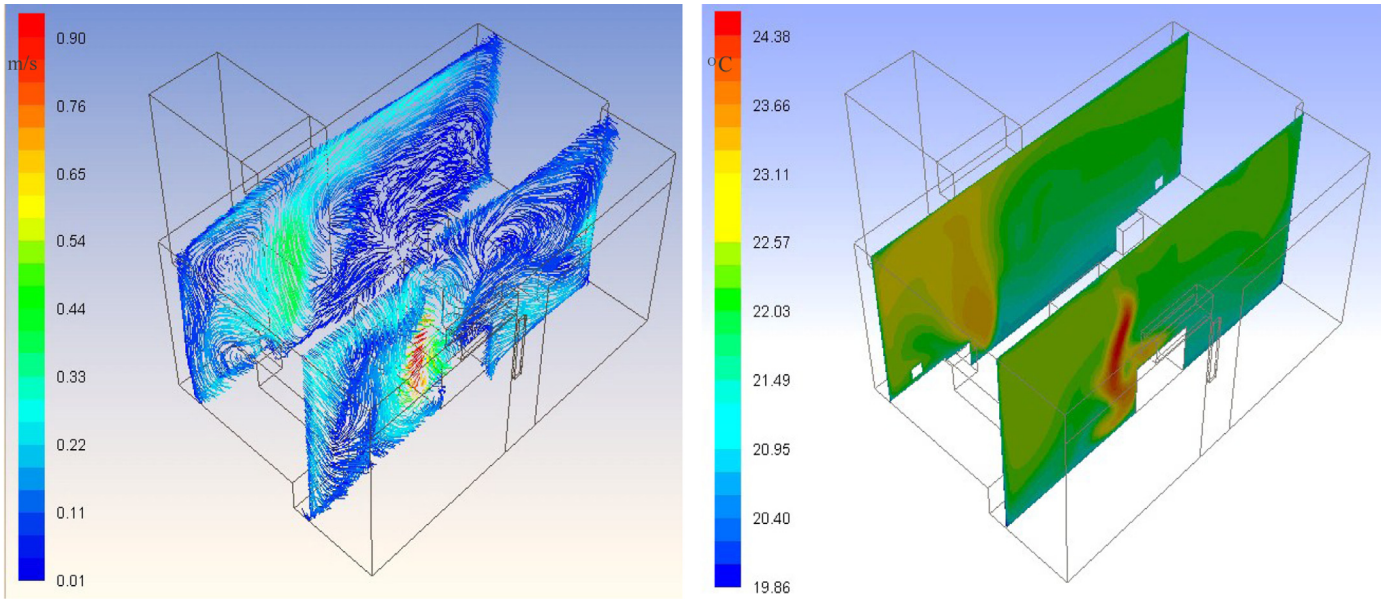

Fig. 7. Streamlines (left) and operative temperature distributions (right) on the sectional vertical plane at y=1 and 3 m.

forced convection condition is prevalent there. Plots of the Fig. 9 show a general increasing trend of the air temperature with height, except of the *p*-3. Indeed, *p*-3 shows its highest temperature equal to 25.1 °C at height 1.3 m, before decreasing with increase of height.

Plots of the Fig. 10 show an irregular trend for variation of the velocity with height. Again here, *p*-1 and *p*-3 give higher values of the velocity at almost all heights. While *p*-2 has the lowest value of the air velocity, namely v=0.015 m/s, *p*-1 at height 1.4 m renders the highest value of the velocity equal to 0.19 m/s. It is also noticeable that *p*-1 undergoes the highest variation of the velocity with height, ranging from 0.04 to 0.19 m/s.

Thermal comfort

In the present study, a MATLAB code has been developed to solve the relevant iterative equations of PMV and PPD. The code acquires the local values of the air velocity and temperature as well as the radiant temperature from the CFD results and calculates the required parameters for evaluation of PMV and PPD, i.e. clothing surface temperature, clothing surface area factor and convective heat transfer coefficient at the body surface. In addition, contours of PMV and PPD have been generated by interpreting the Costume Field Functions in the CFD code.

Fig. 11 presents sectional contours of PMV and PPD on the horizontal plane at z=1.1 m. The figure shows that the "neutral" condition is prevalent in major part of the room at height 1.1 m. It is apparent that, apart from the zone in front of the fan coil, values of the PMV are in acceptable range, namely -0.5 < PMV< +0.5. Accordingly, contours of the PPD demonstrate a percentage range between 4% and 8% for main part of the room at sectional plane. It can be concluded that the central-right-side of the room is the most preferable zone in terms of the PPD, with a percentage lower than 6%.

Values of the PMV and PPD for the regarded positions, namely *p*-1 to *p*-4, are reported in Fig. 12. In order to take into account both reclining (at positions 1 and 2) and sitting postures (at positions 3 and 4), two

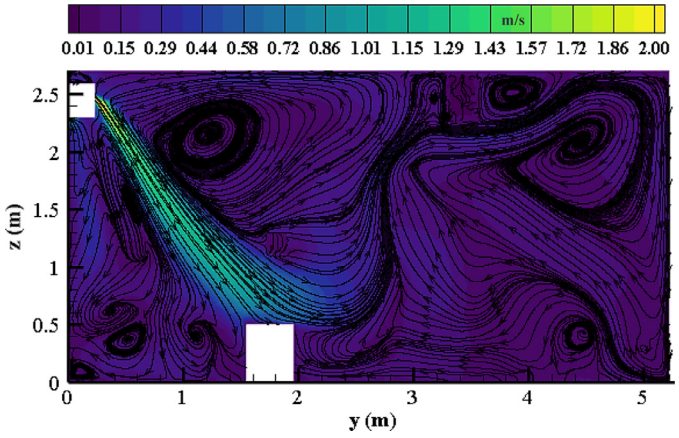

Fig. 8. Air velocity distribution and streamlines on a vertical surface (y-z) crossing the fan coil inlet.

different metabolic rates were considered. At positions 1 and 2 (beds), the metabolic rate was set equal to 0.9 met while at positions 3 and 5 (chairs) it was assumed equal to 1.2 met. The column bars show that a "slightly cool" condition prevails at beds, namely p-1 and p-2. This circumstance for the bed at left-hand side of the room, i.e. p-1, is more severe, with PMV and PPD value equal to -0.61 and 12.8%, respectively. On the other hand, there is a "slightly warm" condition for positions p-3 and p-4 with PMV values 0.26 and 0.11, respectively. It can be seen that all positions satisfy the criteria of the thermal comfort condition, except p-1.

To guarantee the indoor thermal comfort condition, it is necessary to evaluate local discomfort parameters, namely the draught rate (DR), vertical air temperature difference (ΔT), radiant asymmetry (ΔT_{rad}), and floor surface temperature. The draught is defined as an undesirable local cooling of the body caused by air movements. Since the case under study has two velocity inlet vents with rather high turbulence intensity and fluctuations, evaluation of the draught rate is of significant importance.

The draught rate, DR, is estimated based on the local air temperature (T_{air}), local mean air velocity(v_m) and local turbulence intensity (I_t) at neck level, for each occupant. According to ISO 7730 [12], the DR higher than 15% is considered as an unacceptable rate. For the mean velocity

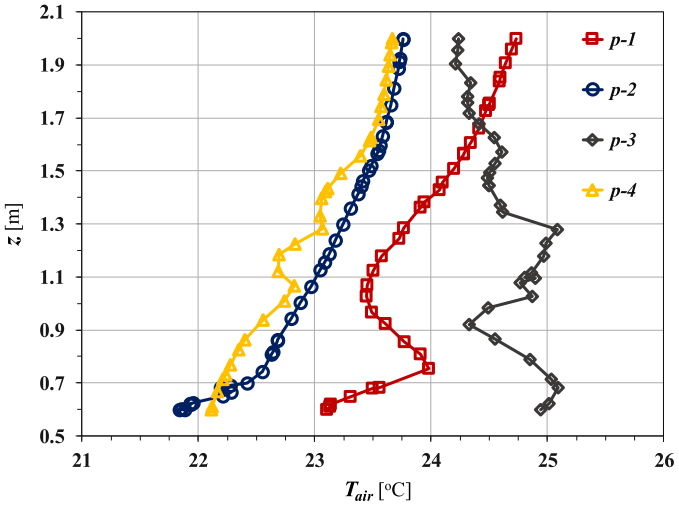

Fig. 9. Air temperature profiles at positions 1–4.

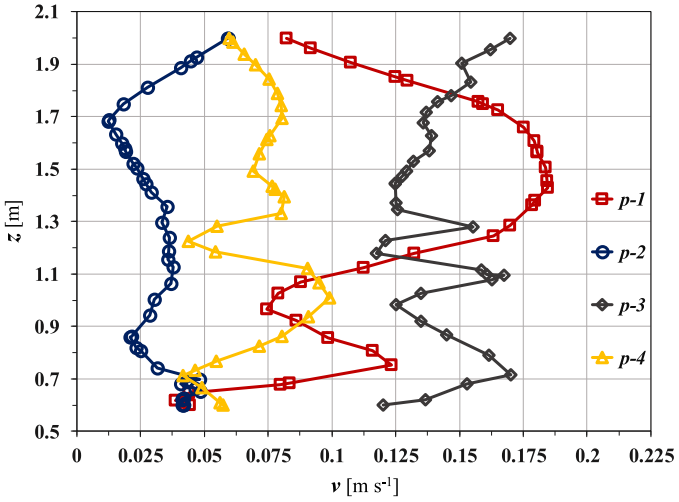

Fig. 10. Air velocity profiles at positions 1–4.

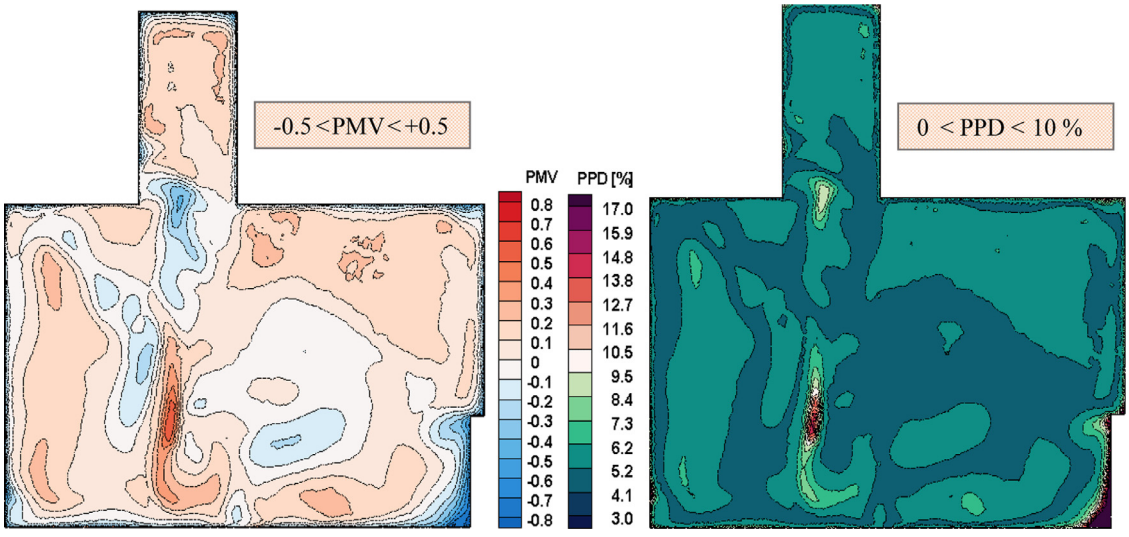

Fig. 11. Contours of the PMV (left) and PPD (right) on a horizontal plane at z=1.1 m.

Table 5
Details of the thermal comfort indices and local discomfort parameters for positions under study.

	T_{air}	T_{rad}	v	I_t	PMV	PPD	DR	ΔT_{air}	ΔT_{rad}
Position	[°C]	[°C]	[m s^{-1}]	%	-	%	%	[°C]	[°C]
p-1	23.09	20.71	0.16	4.54	-0.61	12.8	10.86	-	1.28
p-2	22.61	20.65	0.04	2.71	-0.47	9.61	-	-	1.17
p-3	24.75	20.81	0.13	13.66	+0.26	6.37	9.98	1.61	0.96
p-4	22.75	20.76	0.07	3.53	+0.1	5.21	4.02	0.74	0.73

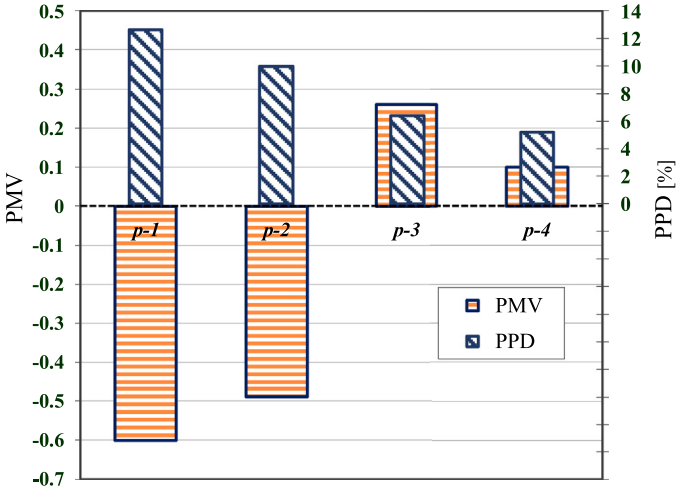

Fig. 12. Thermal comfort indices at positions 1-4.

greater than 0.05 m/s, the *DR* can be calculated by following equation [45, 46]:

$$DR = (34 - T_{air})(v_m - 0.05)^{0.62}(37 \times I_t v_m + 3.14) \quad (24)$$

Fig. 13 illustrates profiles of *DR* on a horizontal plane at two different heights: 1.0 m for a sitting posture and 1.5 m for a standing posture. It should be noted the hollow regions (colourless) in figures represent the zones having mean air velocity lower than 0.05 m/s, where the concept of *DR* is meaningless. The figures at both heights show that the main part of the room is in desired range, namely less than 15%; the profiles varying from dark blue to light blue.

The probable local discomfort caused by the vertical air temperature difference and radiant asymmetry was analysed for positions 1-4. Table 5 reports these indices as well as the relevant parameters for evaluation of the thermal comfort condition. The table shows that the vertical air temperature difference ΔT, between head (z= 1.1 m) and ankles (z= 0.1 m) of the occupants, is below the recommended limit, namely 3 °C [12], for both *p*-3 and *p*-4. Moreover, the radiant temperature asymmetry for all positions is by far lower than allowed value (10 °C), which could be due to the low transmittance of walls and windows.

As mentioned above, only for *p*-1, values of PMV and PPD exceed the allowable range. The results indicate that the preferable location inside the room, in terms of thermal comfort, is *p*-4 with a neutral PMV, the lowest PPD, and a draught rate equal to 4 %. It is also noticeable that the floor surface temperature for the case under study satisfies the required range, i.e. 19°C < T < 29°C.

Fig. 14 shows the influence of indoor humidity on the thermal comfort condition. The chart shows variation of the mean value of PMV on horizontal surface triggered by alteration of the relative humidity, RH. As expected, the simulation results show increase of the PMV value with increase of the indoor humidity. The results indicate that the RH level lower than 40% leads to the "slightly cool" condition in the room.

Local age of the air

The local age of the air is an important index identifying the air quality. It can be used to reflect both freshness and allocation of the breathing air. Figs. 15 and 16 illustrate the contours of the local age of the air, τ, at two typical sectional planes, namely z=1.1 m and z=1.5 m, respectively.

Figures show that the local mean age of the air distributed non-uniformly inside the domain, which could be due to an induced air flow pattern by MVHR and fan coil systems. As expected, values of τ in vicinity of the supply fresh air inlet are significantly lower than other zones, for both sectional planes. On the other hand, the corridor and right upper zone of the room (*p*-2) demonstrate the highest value of the τ inside the room. This situation is more severe for the horizontal plane with 1.5 m height. Furthermore, it can be observed that the younger air was diagonally distributed from the lower right corner to upper left corner, indicating that it takes less time to deliver the fresh air to this region after discharging from the supply vent. The area-weighted average of the τ on horizontal planes z=1.1 m and z=1.5 m render values equal to 5863 s and 5887s, respectively.

In order to make comparisons between different positions and also through the occupied zone, the local age of air τ is normalized by a nominal time constant, defined as the ratio of volumetric fresh air flow, G_f (m^3/s), to the volume of the room V (m^3):

$$\tau^* = \frac{\tau}{V/G_f} \quad (25)$$

The distributions of normalized local age of the air, τ^*, in occupied zone is shown in Fig. 17. The occupied zone, marked in Fig. 1 with red lines, was considered from the floor to the height of 1.80 m. The figure shows that the value of τ^* through the occupied zone varies from 0.94 to 1.02. While the value of τ^* in right-hand side of the occupied zone increase with height, the left-hand side of the domain demonstrates a rather uniform distribution of the τ^*. Such quasi-uniform distribution represents impact of the fan coil airflow on general distribution of the fresh air, hindering to some extent the delivery of the fresh air to left-hand side of the occupied zone.

The Air Change Efficiency (*ACE*) is an indicator of the efficiency and speed of the fresh air exchange inside a domain, employing the theoretical optimum model (piston flow model). It can be defined as a ratio between the shortest possible air change time and the actual air change time. It is evaluated based on the local mean age of the air at exhaust (τ_{out}) and the room-averaged age of the air $\bar{\tau}$:

$$ACE = \frac{\tau_{out}}{2\bar{\tau}} \times 100 \quad (26)$$

According to Eq. (26), a fully mixture of the supply inlet and the exhausted air results in an *ACE* of 50%. For cases with the efficiency higher than 50%, the volumetric air flow can be reduced in order to save the energy. On the contrary, for the cases that *ACE* is lower than normative level, i.e. 50%, the fresh air supply should be increased [9].

Table 6 reports the required parameters to evaluate the Air Change Efficiency (*ACE*), as well as the mean value of τ^* in occupied zone (*OZ*) and values of τ^* at selected positions. Table shows that the value of *ACE* almost meets the normative level of 50%, with just 0.2% insufficiency. It can be observed that the *p*-2 is the worst position in terms of the fresh

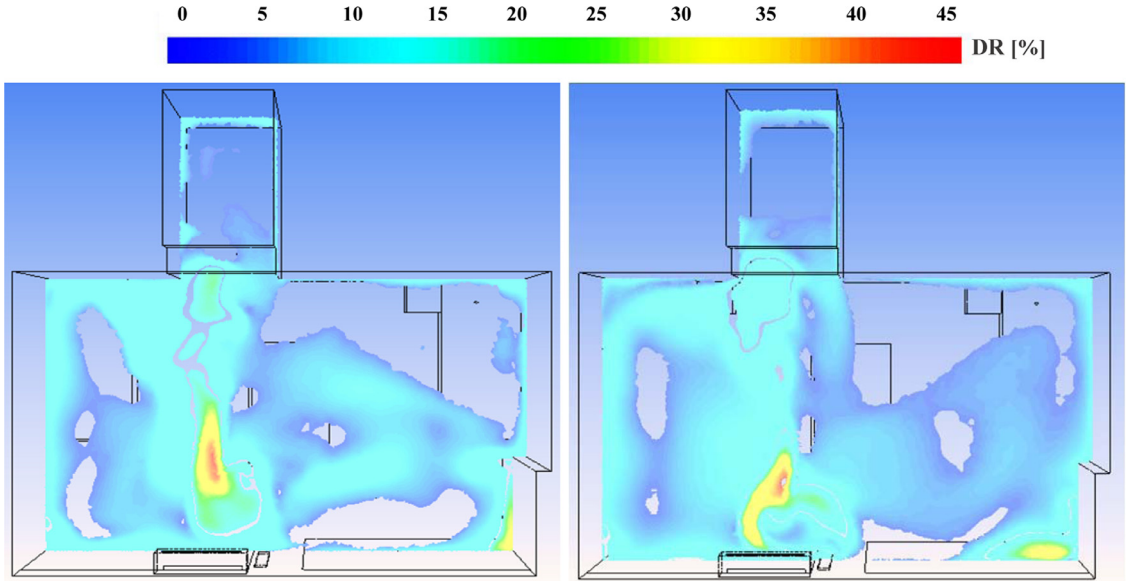

Fig. 13. Profiles of the draught rate (*DR*) on horizontal plane at two heights: 1.0 m (left) and 1.5 m (right).

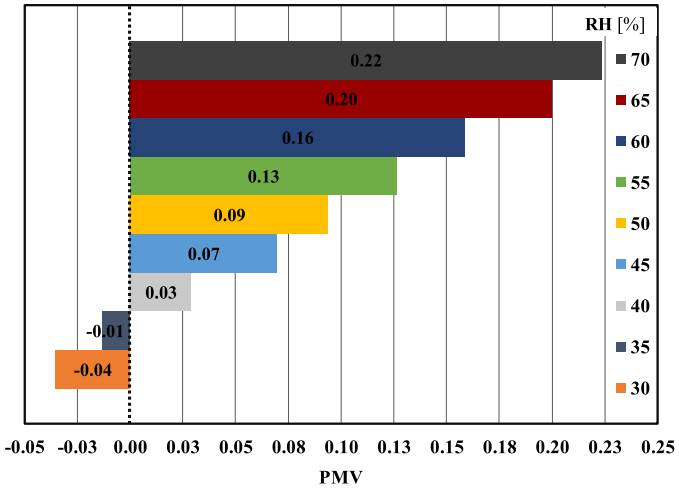

Fig. 14. Mean values of the PMV on horizontal surface at height 1.1 m for different values of the relative humidity.

Table 6
Related parameters to the air change efficiency and values of normalized τ in different zones.

				τ^*			
τ_{out} [s]	$\bar{\tau}$[s]	*ACE* [%]	$\bar{\tau}_{oz}*$	*p*-1	*p*-2	*p*-3	*p*-4
5846	5868	49.81	0.997	0.987	1.021	0.995	0.992

air delivery, compared with other positions, with 2.4% higher value of τ^* with respect to the average of occupied zone. In addition, table shows that the mean age of the air in occupied zone is quasi equal to the average of the age of the air in positions *p*-1 to *p*-4.

VOCs concentration and distribution

The distributions of VOCs, including formaldehyde emission from furniture and toluene emission from painted walls, are presented in Fig. 18, on the typical horizontal plane. In order to interpret and compared better the distribution of contaminants, streamlines of airflow on the same plane are given. The local concentration of *i-th* contaminant is

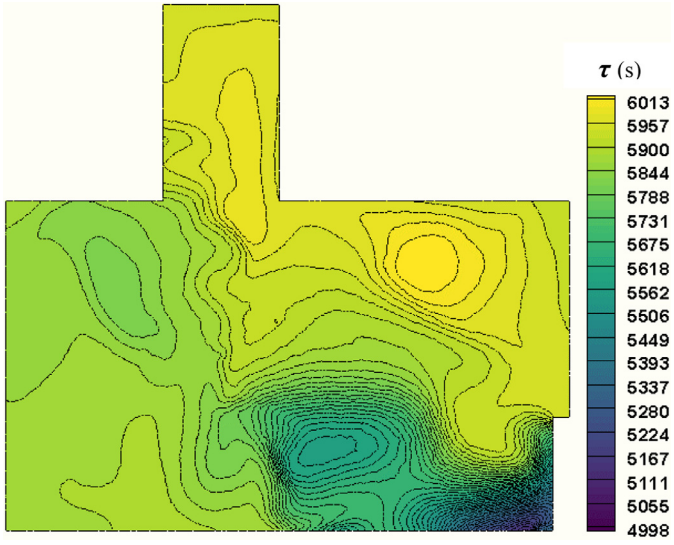

Fig. 15. Contours of the local mean age of the air (s) at height 1.1 m.

expressed in dimensionless form $\tilde{C}_i$, defined as follows:

$$\tilde{C}_i = \frac{G_f \times C_i}{\dot{e}_i} \tag{27}$$

where C_i is the local concentration of *i-th* contaminant (kg/m^3) and $\dot{e}_i$ is the emission rate of *i-th* contaminant at sources (kg/s).

The contours of dimensionless concentration for both VOCs show an non-uniform distribution of gaseous contaminants inside the domain: the lower values of $\tilde{C}_i$in vicinity of supply fresh air vent and significantly higher values of $\tilde{C}_i$in the entrance corridor where the backflow due to large eddies hinder the delivery of fresh air. If one follows the streamlines from the zone adjacent to the supply inlet, one can predict the regions with lower levels of VOCs. Figures show that the dimensionless level of formaldehyde is slightly lower than the toluene on whole domain, which can be due to the different emission sources. Except of the corridor zone, concentration of toluene in vicinity of walls and generally on the left-side of the room is noticeable.

To describe how effective the air supply system is to remove the VOCs, concept of Ventilation Effectiveness (VE) arises. Since gaseous

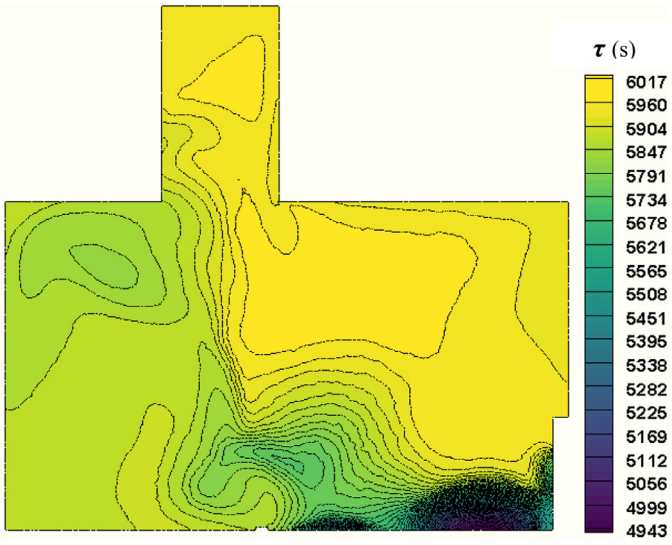

Fig. 16. Contours of the local mean age of the air (s) at height 1.5 m.

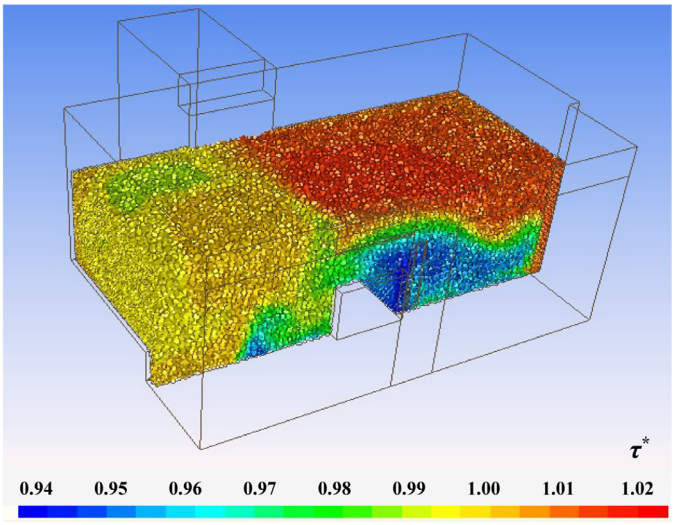

Fig. 17. Distributions of the dimensionless age of the air in occupied zone.

contaminants are usually distributed unevenly inside the room, VE provides a key to the balanced solution because what really matters is the concentration of contaminants at breathing zone. It can be defined as [47]:

$$VE = \frac{C_{outlet}}{C_{bz}} \tag{28}$$

where C_{outlet} is the pollutants concentration at the ventilation outlet and C_{bz} represents the pollutants concentration at breathing zone. For a given ventilation rate combined with a given pollutant emission rate, although the concentration of pollutant at the ventilation outlet is a constant regardless of other conditions due to mass conservation, the concentration of pollutant in breathing zone might be affected by position of pollutant source, interior furniture arrangement, and the details of ventilation system [7].

Fig. 19 demonstrates the ventilation effectiveness and values of $\tilde{C}_i$ at different positions, including *p*-1 to *p*-4, Occupied Zone (*OZ*) and outlet

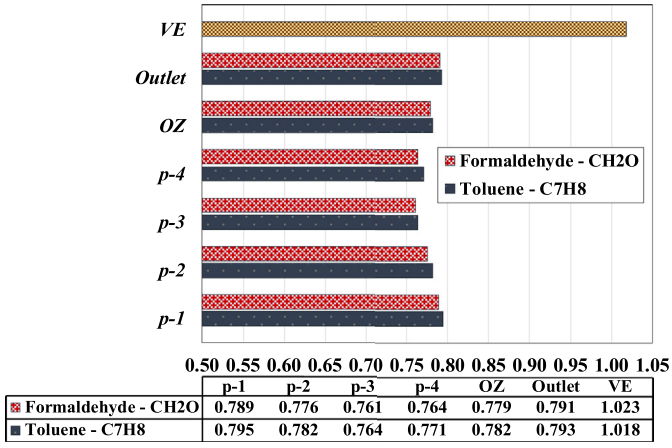

	p-1	p-2	p-3	p-4	OZ	Outlet	VE
Formaldehyde - CH2O	0.789	0.776	0.761	0.764	0.779	0.791	1.023
Toluene - C7H8	0.795	0.782	0.764	0.771	0.782	0.793	1.018

Fig. 19. Ventilation Effectiveness (VE) and dimensionless concentrations of Formaldehyde and toluene.

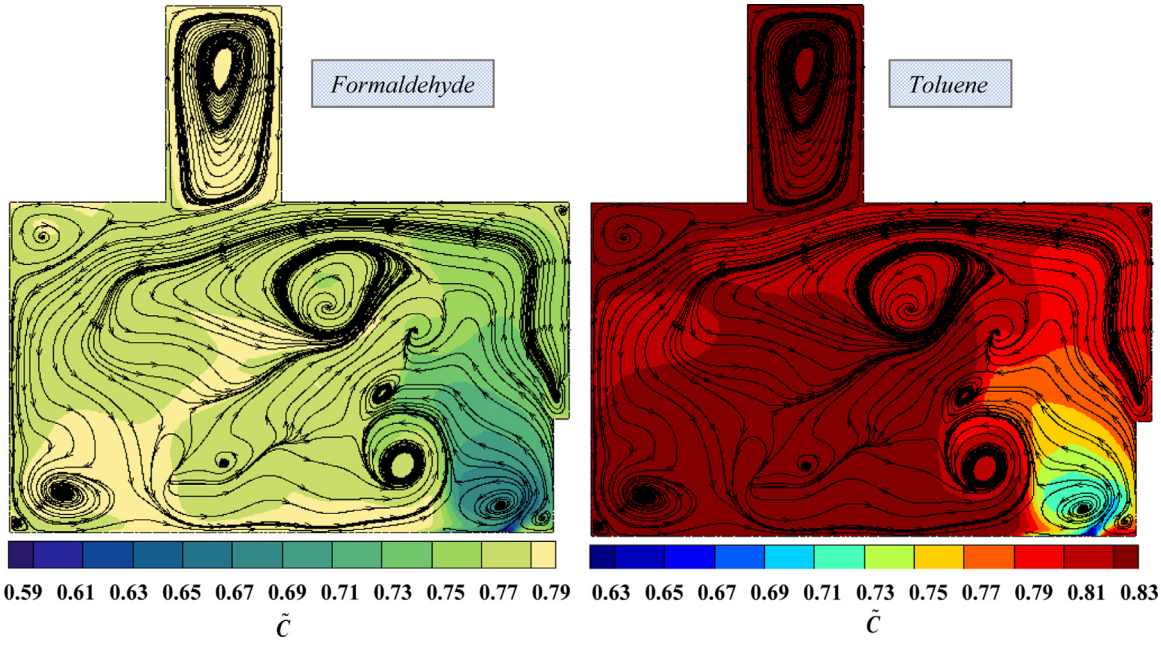

Fig. 18. Distributions of the dimensionless concentration of formaldehyde (left) and toluene (right) with streamlines on the horizontal plane z =1.1 m.

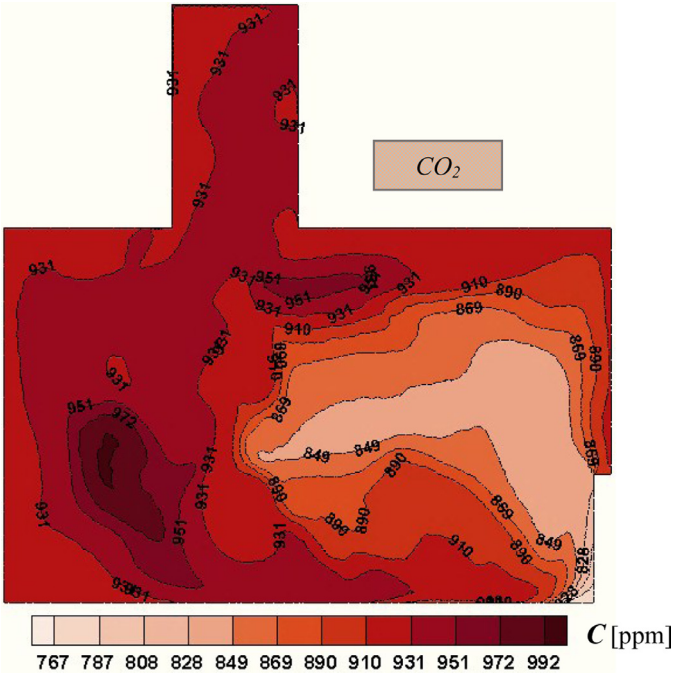

Fig. 20. Contours of the CO_2 concentration (ppm) on the horizontal plane z=1.1 m.

vent. In order to evaluate the contaminant concentration in breathing zone, an average of concentrations at positions p-1 to p-4 was calculated.

The bar chart shows that the concentration of toluene at all positions is slightly higher than formaldehyde. It can be observed that position p-1 has the highest value of VOCs concentration in the breathing zone compared with other positions, with $\tilde{C}_i$ = 0.789 for formaldehyde and $\tilde{C}_i$ = 0.795 for toluene, corresponding to concentrations 2.4210^{-9} and 1.6710^{-7} kg/m^3, respectively. Furthermore, figure shows that the difference between values of the *VE* for each VOC is marginal; slightly higher for the formaldehyde case.

CO_2 concentration field

Contours of the CO_2 concentration in ppm are displayed in Fig. 20. The figure shows a non-uniform distribution of the CO_2 over the domain. On the horizontal plane, the difference between minimum and maximum value of the concentration is about 225 ppm: the minimum concentration is 767 ppm while the maximum value reaches to 992 ppm.

Although the level of the exhaled CO_2 from the occupants was set to the maximum level, the results show that the CO_2 concentration in all zones is lower than the EU prescribed CO_2 indoor levels, i.e. 600 to 1000 ppm above outdoor ambient levels. As expected, the concentration of CO_2 on delivery pathline of the fresh air is lower to significant extent, compared with other zones. Therefore, the right-hand side of the domain has lower level of the CO_2 concentration, which is due the specific layout of the MVHR system (lateral supply air set-up).

Variation of the CO_2 level with height for positions under study, namely p-1 to p-4, is shown in Fig. 21. Plots show a slight variation in concentration with height, except of p-3. Indeed, p-3 plot shows a sudden decrement and again increment between z=1.0 m and z=1.7 m. The reason behind is that position p-3 is located on pathline of the fresh air delivered form the inlet air supply, as shown in Fig. 20. Among four positions, p-1 shows the highest level of CO_2 concentration, varying between 910 and 920 ppm.

Since the upper-left side of the room, in particular p-1, has a high exposure to recirculated airflow exhausting from the fan coil, it can be concluded that such airflow causes the hindrance of the fresh air delivery to this region of the room. As a consequence, the level of gaseous contaminants (VOCs and CO_2) is higher for this region, as presented in Figs. 18–21. Hence, it is interesting to assess effects of the discharged airflow from the fan coil on indoor air quality, which is presented in the following section.

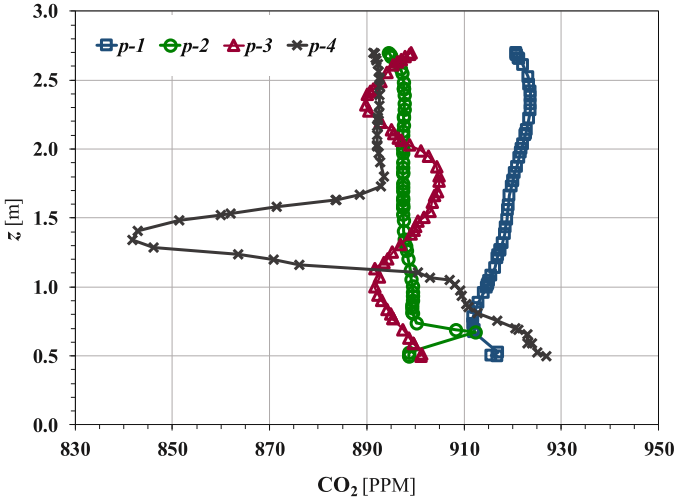

Fig. 21. Variation of the CO_2 concentration (ppm) with height at different positions.

Effects of the fan coil airflow on IAQ and thermal comfort indices

As shown, the airflow exhausted from the fan coil could affect the delivery of the fresh air and distributions of contaminants inside the domain. In order to evaluate such effect on indoor air quality characteristics, four simulations with different working conditions of fan coil were performed; three various air flow rates, i.e. 349 (Min), 427 (intermediate) and 510 (Max) m^3/h, as well as the fan OFF condition. The obtained results showed that while increasing the fan speed (ON mode) would slightly enhance the ventilation efficiency, the OFF mode yields not only a better distribution of the fresh air but also a higher ventilation efficiency than ON mode irrespective of fan speed.

Fig. 22 illustrates delivery of the fresh air as well as the streamlines on horizontal plane at height 1.1 m for both OFF mode and maximum flow rate of the fan coil. The figure shows that the fresh air distribution and streamlines of the OFF mode are by far distinct from when the fan coil operates. The distribution of the local mean age of the air for the maximum flow rate case (on the right) are significantly similar to that of the moderate flow rate, presented in Figs. 15 and 16; a non-uniform distribution of the τ with an airflow field full of counterflows.

On the other hand, contours and streamlines of the OFF mode show a rather uniform distribution of the fresh air within the domain and an airflow field with a general clockwise direction. It can be observed that variation of the τ over the sectional plan for OFF mode case is by far lower than the maximum flow rate case. The figures show that if one set the fan coil OFF, the mean age of the air in entrance corridor would decrease around 500 s, which is due to a better distribution of the fresh air inside the room. It is therefore apparent that the position of the fan coil with respect to the MVHR inlet prevents fresh air from moving throughout the environment. It is also noteworthy to mention that the value of the *ACE* is rather higher when the fan coil is OFF; *ACE* for the fan coil OFF case is 51.1% while for the case with the maximum flow rate is 50.3%.

In order to evaluate impact of the fan coil operation on ventilation efficiency indicators, values of the ventilation efficiency are plotted versus values of the volume flow rate of the fan coil, Q_{fan}, demonstrated in Fig. 23. To determine ventilation efficiency in removal of VOCs, ventilation effectiveness definition was adopted, as presented in Eq. (28). To

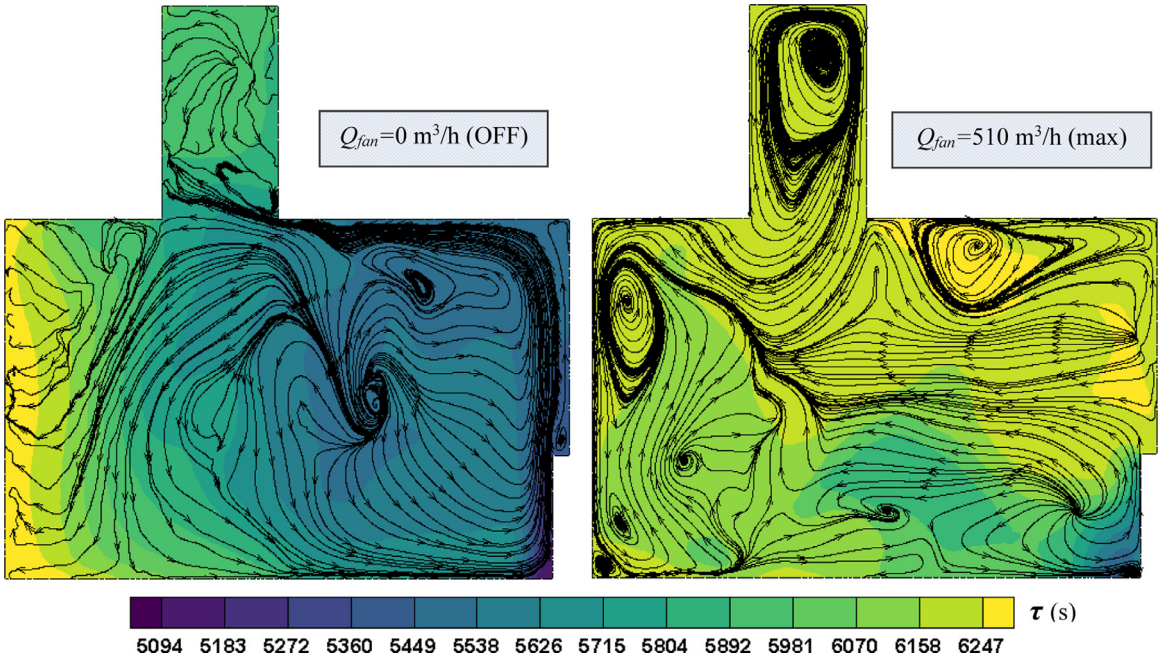

Fig. 22. Distributions of local mean age of the air (s) with streamlines on sectional plane z=1.1 m for OFF condition (left) and maximum speed (right) of the fan coil.

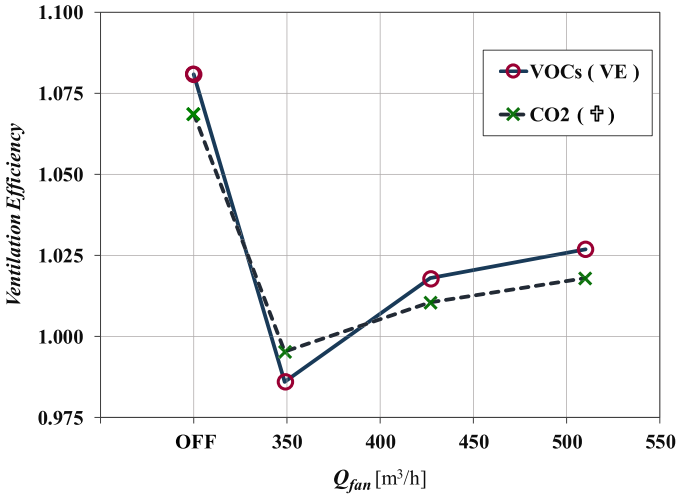

Fig. 23. Ventilation efficiency versus the volume flow rate of the fan coil.

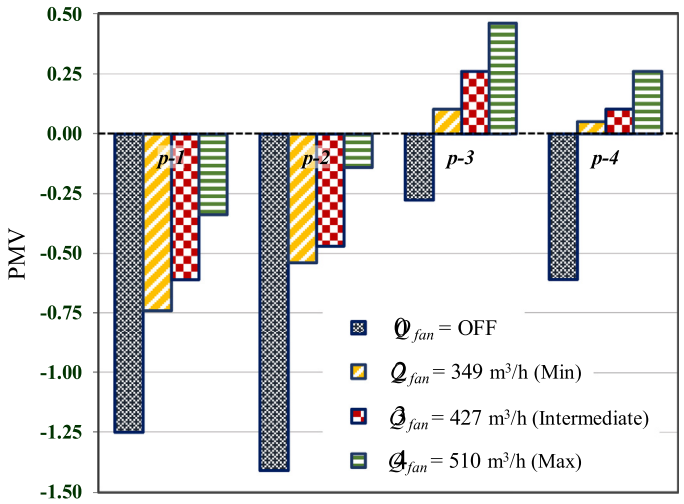

Fig. 24. Impact of the fan coil flow rate on thermal comfort.

have more accurate assessment of the ventilation efficiency in removal of CO_2, another efficiency indicator was taken into account. Due to the fact that the background CO_2 enters the room with fresh air at supply inlet diffuser, the efficiency of ventilation system in removal of CO_2 is determined as below [25, 48]:

$$\Upsilon = \frac{C_{out} - C_{in}}{C_{ave} - C_{in}} \tag{29}$$

where C_{ave} is the averaged indoor CO_2 concentration in steady-state.

In Fig. 23, plots of the *VE* and ϒ demonstrate a rather identical trend with variation of Q_{fan}. The discrepancy between values of the *VE* and ϒ can be considered as negligible, for all volume flow rates. The figure shows that the ventilation efficiency enhances to a small extent by increasing the speed of the fan. However, ventilation efficiency has its highest value when the fan coil is OFF. In comparison with the maximum fan speed case, namely 510 m³/h, the efficiency of the ventilation system is 4.75% higher when the fan coil does not operate.

In fact, ventilation efficiency indices characterise the mixing behaviour of air and the pollutants distribution within a space. Ventilation efficiency is based on an evaluation of the age of the air and also on the concentration distribution of pollutants within the air. In this context, the average age of the air depends on both volumetric flow rate and the airflow pattern. The results presented in Figs. 22 and 23 are good evidence to show how influential the airflow pattern could be on the air change efficiency as well as the ventilation efficiency. This effect is more prominent when the ventilation system is combined with a HVAC system affecting the airflow, as the case under study.

Finally, effects of the fan coil airflow rate on thermal comfort condition is illustrated in Fig. 24. The chart shows variations of PMV in four positions (*p*-1 to *p*-4) triggered by alterations in volume flow rate of fan coil. It can be clearly observed that the operation of fan coil is necessary to maintain acceptable thermal comfort condition, i.e. -0.5 < PMV< +0.5, in four positions, for both reclining (*p*-1 and *p*-2) and sitting (*p*-3 and *p*-4) postures. On the other hand, the figure shows that

switching off the fan coil would deteriorate thermal comfort condition within the room, as expected. This issue is critical since it was shown in Figs. 22 and 23 that the fan coil OFF mode leads to a better distribution of fresh air and ventilation efficiency.

A general solution to this critical condition is alignment of the recirculated flow with fresh airflow in order to minimize the counterflow fields. As shown in Fig. 22, the counterflows, created by crossing the recirculated air and fresh airflow, prevent the perfect delivery of fresh air within the room. Therefore, for spaces conditioning with combined ventilation-recirculation units, it is of significant importance to adjust the direction of the secondary flow (recirculated) with fresh airflow in order to attain simultaneously the best possible ventilation efficiency and thermal comfort condition.

Conclusions

The present study deals with the numerical investigation on efficacy of a coupled MVHR-fan-coil system in providing Indoor Air Quality (IAQ) and thermal comfort inside a student dormitory undergone retrofitting. A Computational Fluid Dynamic (CFD) code was developed by means of finite volume method. The numerical code was validated by comparing the results obtained by simulations with those obtained by experimental measurements. Emissions of the formaldehyde from the furniture and of the toluene from the painted walls were taken into account as the main sources of VOCs inside the domain. In addition, the CO_2 exhaled from occupants were considered as the main indoor source of CO_2.

The results yielded by numerical simulations allowed to analyse the turbulent airflow and operative temperature fields as well as to identify the desirable zones, in terms of thermal comfort and IAQ. Four spots inside the occupied zone were considered as more occupied zones, namely at beds and the desk. The local mean age of the air and distribution of gaseous contaminant concentration, i.e. VOCs and CO_2 concentration, at regarded spots(in breathing zones) and in the occupied zone were studied. Delivery of the fresh air and ventilation efficiency in removal of gaseous contaminants were investigated by evaluating the efficiency indicators such as the air change efficiency, ventilation effectiveness and ventilation efficiency. The results showed that the position *p*-4 is the most preferable position not only in terms IAQ, but also in terms of thermal comfort.

The results indicate that the airflow discharged from the fan coil could have a significant impact on distribution of the fresh air; while it provides a desirable thermal comfort condition within the room, it may hinder to some extent delivery of the fresh air to the occupied zone. To assess such effect, complementary simulations were performed taking into account various volume flow rates of the fan coil as well as the OFF mode. The obtained results showed that increasing the fan speed (ON mode) would slightly enhance the air change efficiency while the OFF mode yields not only a better distribution of the fresh air, but also a higher ventilation efficiency than when the fan coil operates. In comparison with the maximum fan speed case, namely 510 m^3/h, the efficiency of the ventilation system was 4.75% higher when the fan coil did not operate. It was shown that counterflows, created by crossing the recirculated air and fresh airflow, hinder the perfect distribution of fresh air within the room. However, it was observed that switching OFF the fan coil would deteriorate thermal comfort condition to significant extent.

It can be concluded that, for envelopes equipped with a combined HVAC system, in particular coupled ventilation-recirculation units, it is of significant importance to adjust the recirculated flow with fresh airflow in order to minimize the counterflow fields and to attain simultaneously an optimal fresh air distribution and thermal comfort condition. As a direction for future study, conducting an analysis similar to the present study for various positions of the fan coil and MVHR unit inside the envelop would be beneficial since the airflow pattern inside the room, apart from the inlet flow rate, could be affected by the position of HVAC systems.

Declaration of Competing Interests

The authors declare that they have no known competing financial interests or personal relationships that could have appeared to influence the work reported in this paper.

References

[1] J. Fernández-Agüera, S. Domínguez-Amarillo, C. Alonso and F. Martín-Consuegra, "Thermal comfort and indoor air quality in low-income housing in Spain: The influence of airtightness and occupant behaviour," *Energy & Buildings,* vol. 199, p. 102–114, 199.

[2] "The Directive, 2010/31/EU of the European Parliament and of the Council of 19 May 2010 on the Energy Performance of Buildings (EPDB)".

[3] A. Dodoo, L. Gustavsson, R. Sathre, Primary energy implications of ventilation heat recovery in residential buildings, Energy Build. 43 (2011) 1566–1572.

[4] M. Orme, Estimates of the energy impact of ventilation and associated financial expenditures, Energy Build. 33 (3) (2001) 199–205.

[5] E.Z.–. Świercz, Improvement of indoor air quality by way of using decentralised ventilation, J Build. Eng. 32 (2020) 101663.

[6] S. Torresin, G. Pernigotto, F. Cappelletti, A. Gasparella, Combined effects of environmental factors on human perception and objective performance: a review of experimental laboratory works, Indoor Air 28 (4) (2018) 525–538.

[7] R. Zhuang, X. Li, J. Tu, CFD study of the effects of furniture layout on indoor air quality under typical office ventilation schemes, Build. Simul. 7 (2014) 263–275.

[8] C. Buratti, R. Mariani, E. Moretti, Mean age of air in a naturally ventilated office: experimental data and simulations, Energy Build. 43 (2011) 2021–2027.

[9] A. Meiss, J. Feijó-Muñoz, M. García-Fuentes, Age-of-the-air in rooms according to the environmental condition of temperature: a case study, Energy Build. 67 (2013) 88–96.

[10] D. Yang, C. MingMak, Relationships between indoor environmental quality and environmental factors in university classrooms, Build. Environ. 186 (2020) 107331.

[11] ASHRAEASHRAE STANDARD 55. Thermal Environmental Conditions for Human Occupancy, 2013 Atlanta, USA.

[12] "ISO 7730, Moderate thermal environment – Determination of the PMV and PPD indices and specificationof the conditions for thermal comfort, 2005.

[13] P. Fanger, Thermal comfort, analysis and application in environmental engineering, Danish Technical Press, Copenhagen, 1970.

[14] F. Nicol, M. Humphreys, S. Roaf, Adaptive Thermal Comfort: Foundations and analysis, Routledge, NewYork, 2015.

[15] H. Amai, S. Liu, A. Novoselac, Experimental study on air change effectiveness: improving air distribution with all-air heating systems, Build. Environ. 125 (2017) 515–527.

[16] J. Fernández-Agüera, M. Campano, S. Domínguez-Amarillo, I. Acosta, J. Sendra, CO2 Concentration and Occupants' Symptoms in Naturally Ventilated Schools in Mediterranean Climate, Buildings 9 (9) (2019) 197.

[17] F. Mancini, F. Nardecchia, D. Groppi, F. Ruperto, C. Romeo, Indoor environmental quality analysis for optimizing energy consumptions varying air ventilation rates, Sustainability 12 (2020) 482.

[18] J. Jiang, D. Wang, Y. Liu, Y. Di, J. Liu, A field study of adaptive thermal comfort in primary and secondary school classrooms during winter season in Northwest China, Build. Environ. 175 (2020) 106802.

[19] C. Buratti, D. Palladino, Mean Age of Air in Natural Ventilated Buildings: Experimental Evaluation and CO2 Prediction by Artificial Neural Networks, Appl. Sci. 10 (2020) 1730.

[20] G. Semprini, A. Jahanbin, B. Pulvirenti, P. Guidorzi, Evaluation of thermal comfort inside an office equipped with a fan coil HVAC system: A CFD approach, Future Cities Environ. 5 (1) (2019) 1–10.

[21] T. Kobayashi, M. Sandberg, H. Kotani, L. Claesson, Experimental investigation and CFD analysis of cross-ventilated flow through single room detached house model, Build. Environ. 45 (12) (2010) 2723–2734.

[22] A. Awwad, M. Mohamed, M. Fatouh, Optimal design of a louver face ceiling diffuser using CFD to improve occupant's thermal comfort, J. Build. Eng. 11 (2017) 134–157.

[23] A. Poshtiri, S. Mohabbati, Performance analysis of wind catcher integrate dwith shower cooling system to meet thermal comfort conditions in buildings, J. Cleaner Prod. 148 (2017) 452–466.

[24] M. Ning, S. Mengjie, C. Mingyin, P. Dongmei, D. Shiming, Computational fluid dynamics (CFD) modelling of air flow field, mean age of air and CO2 distributions inside a bedroom with different heightsof conditioned air supply outlet, Appl. Energy 164 (2016) 906–915.

[25] X. Ye, Y. Kang, F. Yang, K. Zhong, Comparison study of contaminant distribution and indoor air quality in large-height spaces between impinging jet and mixing ventilation systems in heating mode, Build. Environ. 160 (2019) 106159.

[26] Z. Chen, J. Xin, P. Liu, Air quality and thermal comfort analysis of kitchen environment with CFD simulation and experimental calibration, Build. Environ. 172 (2020) 106691.

[27] A. Jahanbin, G. Semprini, Numerical study on indoor environmental quality in a room equipped with a combined HRV and radiator system, Sustainability 12 (24) (2020) 10576.

[28] G. Ganesh, S. Sinha, T. Verma, Numerical simulation for optimization of the indoor environment of an occupied office building using double-panel and ventilation radiator, J. Build. Eng. 29 (2020) 101139.

[29] J. White, M. Gillott, J. Wood, D. Loveday, K. Vadodaria, Performance evaluation of a mechanically ventilated heat recovery (MVHR) system as part of a series of UK residential energy retrofit measures, Energy Build. 110 (2016) 220–228.
[30] E. Foda, A. El-Hamalawi, J.L. Dréau, Computational analysis of energy and cost efficient retrofitting measures for the French house, Build. Environ. 175 (2019) 106792.
[31] M. Assimakopoulos, R.D. Masi, A. Fotopoulou, D. Papadaki, S. Ruggiero, G. Semprini, G. Vanoli, Holistic approach for energy retrofit with volumetric add-ons toward nZEB target: Case study of a dormitory in Athens, Energy Build. 207 (2020) 109630.
[32] Q. Chen, Comparison of different k-e models for indoor airflow computations, Numer. Heat Transfer Part B 28 (1999) 4391–4409.
[33] A. Jahanbin, E. Zanchini, Effects of position and temperature-gradient direction on the performance of a thin plane radiator, Appl. Therm. Eng. 105 (2016) 467–473.
[34] H. Versteeg, W. Malalasekera, An introduction to computational fluid dynamics: the finite volume method, 2nd ed., Pearson - Prentice Hall, 2007.
[35] P. Tsilingiris, Thermophysical and transport properties of humid air attemperature range between 0 and 100oC, Energy Convers. Manage. 49 (2008) 1098–1110.
[36] K. Raznjevic, Handbook of Thermodynamic Tables & Charts, McGraw-Hill, 1976.
[37] Q. Zhao, Z. Lian, D. Lai, Thermal comfort models and their developments: a review, Energy Built Environ. 2 (1) (2020) 21–33.
[38] V. Chanteloup, P. Mirade, Computational fluid dynamics (CFD) modelling of local mean age of air distribution in forced-ventilation food plants, J. Food Eng. 90 (2009) 90–103.
[39] G. Gan, Effective depth of fresh air distribution in rooms with single-sided natural ventilation, Energy Build. 31 (2000) 65–73.
[40] N.B. Goodman, A. Wheeler, P. Paevere, P. Selleck, M. Cheng, A. Steinemann, Indoor volatile organic compounds at an Australian university, Build. Environ. 135 (2018) 344–351.
[41] K. Kim, S. Kim, H. Kim, J. Park, Formaldehyde and TVOC emission behaviors according to finishing treatment with surface materials using 20 L chamber and FLEC, J. Hazard. Mater. 177 (2010) 90–94.
[42] T. Salthammer, Data on formaldehyde sources, formaldehyde concentrations and air exchange rates in European housings, Data Brief 22 (2019) 400–435.
[43] L. Tian, Z. Lin, Q. Wang, Comparison of gaseous contaminant diffusion under stratum ventilation and under displacement ventilation, Build. Environ. 45 (2010) 2035–2046.
[44] Q. Chen, J. Srebic, A procedure for verification, validation, and reporting of indoor environment CFD analyses, HVAC R Res. 8 (2) (2002) 201–216.
[45] P. Fanger, A. Melikov, H. Hanzawa, J. Ring, Air turbulence and sensation of draught, Energy Build. 12 (1988) 21–39.
[46] H. Koskela, J. Heikkinen, R. Niemelä, T. Hautalampi, Turbulence correction for thermal comfort calculation, Build. Environ. 36 (2) (2001) 247–255.
[47] D. Rim, A. Novoselac, Ventilation effectiveness as an indicator of occupant exposure to particles from indoor sources, Build. Environ. 45 (2010) 1214–1224.
[48] K. Chung, S. Hsu, Effect of ventilation pattern on room air and contaminant distribution, Build. Environ. 36 (2001) 989–998.